

Identification of a Novel *FGFRL1* MicroRNA Target Site Polymorphism for Bone Mineral Density in Meta-Analyses of Genome-Wide Association Studies

Tianhua Niu^{1,§}, Ning Liu^{2,§}, Ming Zhao¹, Guie Xie², Lei Zhang^{1,3}, Jian Li¹, Yu-Fang Pei¹, Hui Shen¹, Xiaoying Fu¹, Hao He¹, Shan Lu², Xiang-Ding Chen², Li-Jun Tan², Tie-Lin Yang⁴, Yan Guo⁴, Paul J. Leo⁵, Emma L. Duncan^{5,6}, Jie Shen⁷, Yan-Fang Guo⁷, Geoffrey C. Nicholson⁸, Richard L. Prince^{9,10}, John A. Eisman¹¹, Graeme Jones¹², Philip N. Sambrook¹³, Xiang Hu², Partha M. Das¹, Qing Tian¹, Xue-Zhen Zhu³, Christopher J. Papasian¹⁴, Matthew A. Brown⁵, André G. Uitterlinden^{15,16,17}, Yu-Ping Wang^{1,18}, Shuanglin Xiang^{*,2}, Hong-Wen Deng^{1*,2}

¹Center for Bioinformatics and Genomics, Department of Biostatistics and Bioinformatics, Tulane University School of Public Health and Tropical Medicine, New Orleans, LA 70112, USA

²Key Laboratory of Protein Chemistry and Developmental Biology of State Education Ministry of China, College of Life Sciences, Hunan Normal University, Changsha, Hunan 410081, P. R. China

³Center of System Biomedical Sciences, University of Shanghai for Science and Technology, Shanghai 200093, P. R. China

⁴Laboratory of Biomedical Information Engineering of Ministry of Education, and Institute of Molecular Genetics, School of Life Science and Technology, Xi'an Jiaotong University, Xi'an, Shaanxi 710049, P. R. China

⁵Human Genetics Group, University of Queensland Diamantina Institute, Translational

Research Institute, Princess Alexandra Hospital, Brisbane, Queensland, Australia

⁶Department of Diabetes and Endocrinology, Royal Brisbane and Women's Hospital,
Brisbane, Queensland, Australia

⁷Third Affiliated Hospital of Southern Medical University, Guangzhou, Guangdong, P. R.
China

⁸Rural Clinical School, The University of Queensland, Toowoomba, Australia

⁹School of Medicine and Pharmacology, University of Western Australia, Perth, Australia

¹⁰Department of Endocrinology and Diabetes, Sir Charles Gairdner Hospital, Perth, Australia

¹¹Garvan Institute of Medical Research, University of New South Wales, Sydney, Australia

¹²Menzies Research Institute, University of Tasmania, Hobart, Australia

¹³Kolling Institute, Royal North Shore Hospital, University of Sydney, Sydney, Australia

¹⁴Department of Basic Medical Science, University of Missouri-Kansas City, Kansas City,
USA

¹⁵Department of Internal Medicine, Erasmus Medical Center, Rotterdam, The Netherlands

¹⁶Department of Epidemiology, Erasmus Medical Center, Rotterdam, The Netherlands

¹⁷Netherlands Genomics Initiative (NGI)-sponsored Netherlands Consortium for Healthy
Aging (NCHA), Leiden, The Netherlands

¹⁸Department of Biomedical Engineering, Tulane University, New Orleans, LA, 70118, USA

*To whom correspondence should be addressed at: Hong-Wen Deng, Ph.D., Professor and
Edward G. Schlieder Endowed Chair, Department of Biostatistics and Bioinformatics,
Director, Center for Bioinformatics and Genomics, Tulane University School of Public Health

and Tropical Medicine, 1440 Canal Street, Suite 2001, New Orleans, LA 70112, USA. Tel: 504-988-1310; Fax: 504-988-1706; Email: hdeng2@tulane.edu or Shuanglin Xiang, Ph.D., Professor and Director, Key Laboratory of Protein Chemistry and Developmental Biology of State Education Ministry of China, Dean, College of Life Sciences, Hunan Normal University, Changsha, Hunan 410081, P. R. China. Tel: +86-731-8887-2095; Fax: +86-731-8887-2792; Email: xshlin@hunnu.edu.cn

§These authors contributed equally to the work

ABSTRACT

MicroRNAs (miRNAs) are critical post-transcriptional regulators. Based on a previous genome-wide association (GWA) scan, we conducted a polymorphism in microRNAs' Target Sites (poly-miRTS)-centric multistage meta-analysis for lumbar spine (LS)-, total hip (HIP)-, and femoral neck (FN)-bone mineral density (BMD). In stage I, 41,102 poly-miRTSs were meta-analyzed in 7 cohorts with a genome-wide significance (GWS) $\alpha = 0.05/41,102 = 1.22 \times 10^{-6}$. By applying $\alpha = 5 \times 10^{-5}$ (suggestive significance), 11 poly-miRTSs were selected, with *FGFRL1* rs4647940 and *PRR5* rs3213550 as top signals for FN-BMD (P-value = 7.67×10^{-6} and 1.58×10^{-5}) in gender-combined sample. In stage II *in silico* replication (two cohorts), *FGFRL1* rs4647940 was the only signal marginally replicated for FN-BMD (P-value = 5.08×10^{-3}) at $\alpha = 0.10/11 = 9.09 \times 10^{-3}$. *PRR5* rs3213550 was also selected based on biological significance. In stage III *de novo* genotyping replication (two cohorts), *FGFRL1* rs4647940 was the only signal significantly replicated for FN-BMD (P-value = 7.55×10^{-6}) at $\alpha = 0.05/2 = 0.025$ in gender-combined sample. Aggregating three stages, *FGFRL1* rs4647940 was the *single* stage I-discovered and stages II- and III-replicated signal attaining GWS for FN-BMD (P-value = 8.87×10^{-12}). Dual-luciferase reporter assays demonstrated that *FGFRL1* 3' untranslated region harboring rs4647940 appears to be hsa-miR-140-5p's target site. In a zebrafish microinjection experiment, dre-miR-140-5p is shown to exert a dramatic impact on craniofacial skeleton formation. Taken together, we provided functional evidence for a novel *FGFRL1* poly-miRTS rs4647940 in a previously known 4p16.3 locus, and experimental and clinical genetics studies have shown both *FGFRL1* and hsa-miR-140-5p are important for bone formation.

INTRODUCTION

Osteoporosis, a common skeletal disease characterized by low bone mineral density (BMD) and deterioration in bone microarchitecture, impaired bone strength and leads to an increased risk of fragility fractures (1). Twin and family studies of BMD have shown that 60-90% of BMD variation can be attributed to genetic factors (2-6).

MicroRNAs (miRNAs) are evolutionarily conserved, endogenous, single-stranded, noncoding RNAs of 18—24 nucleotides in length that regulate gene expression, typically by binding to their complementary sequences located at 3' untranslated regions (UTRs) of target mRNAs by mediating target mRNA degradation and/or protein synthesis repression (7, 8). There are 2,578 mature human miRNA sequences currently listed in miRBase (9, 10). Further, more than 45,000 conserved miRNA target sites within human 3' UTRs have been identified, and more than 60% of human protein-coding genes are under selective pressure to maintain pairing to miRNAs (11). Each miRNA can modulate about 200 target mRNAs (12, 13).

Canonical miRNA targeting is mediated by a perfect Watson-Crick pairing of miRNA's 5' seed region, typically comprising nucleotides 2–7 at 5'-end of an miRNA (12), which determines both target site specificity (14-16) and most of energy change involved in miRNA-mRNA binding (17, 18). Some 6-mer seeds also match to positions 1–6 (19, 20). The miRNA-mRNA binding is determined not only by the thermodynamic property of miRNA, but also by characteristic secondary structure of the target mRNA's 3' UTR containing the miRNA binding site (21), which can be affected by single nucleotide polymorphisms (SNPs)

either inside or outside the miRNA target site that alter miRNA accessibility (13, 22).

Disruptions of miRNA binding sites by SNPs present in 3' UTRs of mammalian genes known as polymorphisms in microRNAs Target Sites (poly-miRTSs), have been clearly documented [e.g., (23-25)]. By *abolishing/modifying/creating* miRNA target sites, such SNPs may affect target mRNA/protein expressions, which could modulate diseases risks (23, 26-28).

Although genome-wide association (GWA) studies have been successful in identifying new genes with common variants that exert modest effects on complex traits (e.g., BMD), conventional “hypothesis-free” GWA approach commonly performs 1 million independent association tests, and therefore has strict requirements for controlling occurrences of false positives in such an “unbiased” approach [typically, a genome-wide significance (GWS) threshold of $\alpha = 5 \times 10^{-8}$ is applied], resulting in severe multiple testing corrections. True positive associations could be missed, particularly in the presence of limited replication resources (29). More than 90% of SNPs collected in the National Human Genome Research Institute (NHGRI) Genome-wide Association Study catalog (30) are located within non-coding regions (31). However, many such non-coding SNPs are simply neglected due to a lack of functional annotations. Therefore, revisiting GWA scans from the perspective of biological knowledge (e.g., miRNA target sites, promoter methylation regions) could discover new genetic variants that are *experimentally testable*. Because the human genome harbors a large number of poly-miRTSs that are potentially important (32, 33), screening exclusively those poly-miRTSs could discover novel regulatory SNPs affecting gene expressions thanks

to a less number of statistical tests based on biological meaning. Because such a functional candidate genomic region association approach may increase type I error rate (i.e., α), to minimize false positives, a multi-stage approach was applied, such that those stage I-selected poly-miRTSs based on a moderate threshold ($\alpha = 5 \times 10^{-5}$) are subject to stringent stage II and stage III independent replications based on their respective Bonferroni-corrected significance thresholds.

RESULTS

Basic genotype information and phenotype characteristics for the three stages of GWA meta-analysis focusing on poly-miRTSs were presented in Table 1.

Stage I (GWA Discovery)

As shown in Fig. 1, seven cohorts (i.e., OOS, KCOS, COS, FHS, IFS, WHI-AA, and WHI-HIS) were included in this GWA discovery stage. Through genotype imputation using 1KG reference panels, 5,842,825 SNPs (genotyped + imputed) were imputed (34). Because the current study only focused on 41,102 poly-miRTSs of 5,842,825 SNPs, quantile-quantile (Q-Q) plots were generated exclusively for these 41,102 poly-miRTSs for gender-combined (i.e., male and female) sample and female-specific sample, respectively (Supplementary Material, Fig. S1). SNP ranks, names, and P-values for five top signals of 11 stage I-selected poly-miRTS for FN-BMD in gender-combined sample (i.e., rs4647940, rs3213550, rs523200, rs11581122, and rs10739677) and in female-specific sample (i.e., rs4647940, rs1599795, rs10739677, rs3213550, and rs523200) were indicated. After adjusting BMD phenotypes by

five principal components, genomic control (GC) inflation factor (λ_{GC}) was computed for each of lumbar spine (LS)-, total hip (HIP)-, and femoral neck (FN)-BMD traits for stage I 41,102 poly-miRTSs in gender-combined and female-specific samples, respectively, and these λ_{GC} 's were compared with those of 5,842,825 SNPs of the traditional GWA study of Zhang et al. (2014) (34). Overall, because these 41,102 poly-miRTSs were not random SNPs, but rather SNPs with biologically higher prior probabilities, λ_{GC} 's were slightly increased from the range of 1.03–1.04 to the range of 1.033–1.121 (Supplementary Material, Table S1). To protect against an increase in type I error rate (i.e., α), we applied a multi-stage approach such that those stage I-selected poly-miRTSs based on a moderate threshold ($\alpha = 5 \times 10^{-5}$) are subject to stage II and stage III independent replications based on their respective Bonferroni-corrected significance thresholds. Three poly-miRTSs of two genes attained GWS (i.e., $\alpha = 0.05/41,102 = 1.22 \times 10^{-6}$): *OSBPL2* rs6089342 (P-value = 2.70×10^{-7}) and rs6121978 (P-value = 3.65×10^{-7}) located on chromosome 20q13.33 for LS-BMD in gender-combined sample, and *TMEM135* rs550773 (P-value = 5.93×10^{-7}) located on chromosome 11q14.2 for FN-BMD in gender-combined sample. Another 37 poly-miRTSs had P-values in the range of 1.22×10^{-6} to 5×10^{-5} . Of these 40 top-ranking poly-miRTSs at $\alpha = 5 \times 10^{-5}$ (suggestive significance), 11 (i.e., *SLC22A2* rs3127592 and rs3127593, *FGFRL1* rs4647940, *CD80* rs1599795, *C6orf97-ESR1* rs9479085, *PRR5* rs3213550, *PTH2R* rs1057392, *FAM125B* rs10739677, *AMAC1* rs17547201, *FAM46C* rs11581122, and *SFI* rs523200, located in 10 gene regions) were selected based on SNP selection criteria: (i) statistical significance threshold (P-value $< 5 \times 10^{-5}$), (ii) allelic association direction (if ≥ 2 traits are available, same directions for ≥ 6 of 7 cohorts for each trait; if only 1 trait is available, same directions for all 7 cohorts), and (iii) biological

significance [i.e., being an miRNA target site disease-associated SNP (miRTSdSNP)

according to Bruno et al. (35)].

Stage II (*in silico* Replication)

At stage II, these above 11 stage I-selected poly-miRTSs were further subject to *in silico* replication in two independent cohorts: (i) RS ($N=4,904$, 57.0% women), and (ii) AOGC ($N=1,955$, 100.0% women). The following SNP selection criteria were applied for stage II SNP selection: (i) statistical significance threshold (Bonferroni-corrected marginal significance, i.e. $P\text{-value} < 0.1/11 = 9.09 \times 10^{-3}$), and (ii) biological significance. Only one poly-miRTS met statistical significance threshold — *FGFRL1* rs4647940, with a $P\text{-value} = 5.078 \times 10^{-3}$ for FN-BMD in gender-combined sample (Table 2). At stage I, *FGFRL1* rs4647940 is top signal among these stage I-selected 11 poly-miRTSs for FN-BMD in gender-combined sample. As shown in Supplementary Material, Fig. S1A, for this trait, there was a bigger gap of $-\log_{10}(P\text{-value})$ between rs3213550 and rs523200 [$\Delta\text{-log}_{10}(P\text{-value}) = -\log_{10}(1.58 \times 10^{-5}) + \log_{10}(4.76 \times 10^{-5}) = 0.4789$] than between rs523200 and rs11581122 [$\Delta\text{-log}_{10}(P\text{-value}) = -\log_{10}(4.76 \times 10^{-5}) + \log_{10}(6.66 \times 10^{-5}) = 0.1459$], and between rs11581122 and rs10739677 [$\Delta\text{-log}_{10}(P\text{-value}) = -\log_{10}(6.66 \times 10^{-5}) + \log_{10}(1.267 \times 10^{-4}) = 0.2793$]. In addition, as shown in Supplementary Material, Fig. S1B, second top signal for FN-BMD trait in female-specific sample, i.e., rs1599795, had a less significant $P\text{-value}$ (i.e., 8.32×10^{-5}) than the $P\text{-value}$ of second top signal (i.e., 1.58×10^{-5}) for the same trait in gender-combined sample, i.e. rs3213550. Further, besides rs4647940 ($P\text{-value} = 7.67 \times 10^{-6}$), which attained an $\alpha = 5 \times 10^{-5}$ threshold in gender-combined and female-specific samples, rs3213550 ($P\text{-value} = 1.58 \times 10^{-5}$)

is the only other poly-miRTS that attained an $\alpha = 5 \times 10^{-5}$ threshold in gender-combined sample, and an $\alpha = 5.5 \times 10^{-4}$ (a more relaxed threshold compared to $\alpha = 5 \times 10^{-5}$) in female-specific sample, respectively. Taken together, at stage II, *PRR5* poly-miRTS rs3213550 exhibited a relatively robust association for FN-BMD at stage I. Although this SNP did not reach stage II marginal significance threshold ($P\text{-value} = 0.3138 > 9.09 \times 10^{-3}$), it is notable that at stage I, it had consistent significant associations for FN-BMD in gender-combined and female-specific samples. *PRR5* is a recently identified component of mammalian target of rapamycin complex 2 (mTORC2), which also contains four other components, i.e. mTOR, Rictor, mSin1, mLST8/GL and plays a critical role in bone development and homeostasis (36-38). *PRR5* interacts with Rictor in regulating skeletal growth (39). Further, prior biological evidence suggests that rs3213550, which is located in 3' UTR of *PRR5* gene, is a disease-associated miRTSdSNP (35). Therefore, at stage II, based on biological significance of *PRR5* and mTORC2 for bone growth and stage I statistical significance for FN-BMD (i.e., a runner up following rs4647940), *PRR5* poly-miRTS rs3213550 was also selected for stage III *de novo* replication.

Stage III (*de novo* Genotyping Replication)

At stage III, the above two stage II-selected poly-miRTSs located in two respective gene regions — *FGFRL1* and *PRR5*, were further subject to replication by *de novo* genotyping in two independent cohorts: (i) KCOSR ($N=3,923$, 57.6% women), and (ii) COSR ($N=2,740$, 57.7% women). In this stage, SNP selection criterion is solely based on Bonferroni-corrected statistical significance threshold ($P\text{-value} < 0.05/2=0.025$) for FN-BMD trait in gender-

combined sample. Only *FGFRL1* rs4647940 met this criterion for FN-BMD (P-value = 7.55×10^{-6}), in gender-combined sample (Table 2).

Stage I+II+III Meta-analysis

Meta-analysis results pooling all available data across stages I, II, and III for two poly-miRTSs — *FGFRL1* rs4647940 and *PRR5* rs3213550 for FN-BMD in gender-combined sample revealed that *FGFRL1* rs4647940 (P-value = 8.87×10^{-12}) was the only poly-miRTS that attained both the current study's GWS (i.e., P-value $< 1.22 \times 10^{-6}$) and conventional GWS (i.e., P-value $< 5 \times 10^{-8}$) (Table 2). Stage I's second top signal for FN-BMD of 11 stage I-selected poly-miRTSs — *PRR5* rs3213550 (P-value = 1.17×10^{-5}) did not attain the current study's reduced GWS. Taken together, the current study has identified and robustly replicated *FGFRL1* rs4647940 as the only signal associated with FN-BMD in gender-combined sample. As shown in forest plot of stage I+II+III meta-analysis of poly-miRTS, *FGFRL1* rs4647940 for FN-BMD in gender-combined sample (Fig. 2), not only the overall meta-analysis across these 11 cohorts attained conventional GWS (i.e., P-value $< 5 \times 10^{-8}$), but also all replication cohorts of stage II (AOGC and RS) and stage III (COSR and KCOSR) have same directions of allelic associations as ≥ 6 out of 7 stage I cohorts.

Regional Association Plots and Linkage Disequilibrium (LD) r^2 Plots

A regional association plot of traditional GWA meta-analysis results for FN-BMD trait of *FGFRL1* poly-miRTS rs4647940 and those stage I SNPs in the ± 100 -kb flanking regions, particularly intergenic rs6827815 (currently considered as located within *IDUA* gene region;

http://www.ncbi.nlm.nih.gov/projects/SNP/snp_ref.cgi?rs=6827815) of Zhang et al. (34) and *IDUA* rs3755955 of Estrada et al. (40), were shown in Fig. 3A, with a zoom-in view of the middle part (i.e., ± 27 -kb flanking regions) spanning these three SNPs shown in Fig. 3B. In order to delineate a high-resolution LD structure for 4p16.3 locus encompassing these three SNPs, an LD r^2 plot for 58 SNPs (from rs11731377 to rs13114658 spanning 80.744-kb) was generated for OOS (Fig. 4A) and KCOS (Fig. 4B) cohorts, respectively, both of which are of Caucasian ancestry. This entire region is partitioned into left and right haplotype blocks: block 1 (left) extends from rs11731377 to rs4647940 (30 SNPs), and block 2 (right) extends from rs13137819 and rs13114658 (28 SNPs) in each cohort. All these three SNPs (i.e., rs3755955, rs6827815, and rs4647940) are located within block 1 in both cohorts, such that rs4647940 is in a *moderately high* LD with both rs3755955 [$r^2 = 0.649$ and 0.842 for OOS ($N=987$) and KCOS ($N=2,250$), respectively] and rs6827815 ($r^2 = 0.702$ and 0.857 in OOS and KCOS, respectively).

Conditional Meta-analysis

In rs3755955-rs6827815-rs4647940 region, because rs6827815 (distance: 20.946 kb) is physically closer to rs4647940 than rs3755955 (distance: 25.977 kb), two conditional analyses were performed: (i) rs4647940 conditional on rs6827815: under a fixed-effects model, $P\text{-value} = 1.35 \times 10^{-3}$ for FN-BMD in stage I gender-combined sample, which remains to be significant at $\alpha = 5.00 \times 10^{-3}$, suggesting rs4647940 and rs6827815 represent distinct signals at this chromosomal locus, and (ii) rs4647940 conditional on both rs3755955 and rs6827815: under a fixed-effects model, $P\text{-value} = 1.33 \times 10^{-3}$ for FN-BMD in stage I gender-

combined sample.

Predicted RNA Secondary Structures of *FGFRL1* 3' UTR Harboring rs4647940

The secondary structure of a 121-bp (i.e., rs4647940 with ± 60 -bp flanking regions) *FGFRL1* 3' UTR segment carrying either wild-type (WT) (i.e., "C") or mutant (MUT) (i.e., "G") allele of rs4647940 was predicted by RNAfold. Difference of minimum free energies (MFEs) between folding patterns for MUT and WT alleles is $\Delta\text{MFE} = \text{MFE}_{\text{MUT}} - \text{MFE}_{\text{WT}} = (-34.30) - (-34.10) = -0.20$ kcal/mol. Therefore, the secondary structure of WT allele such that the SNP is located in a stem connected to a terminal loop and an internal loop (Fig. 5A) is less stable than that of MUT allele such that the SNP is located in a stem connected to two internal loops (Fig. 5B). Therefore, this SNP causes a change of RNA secondary structure of *FGFRL1* 3' UTR, potentially affecting miRNA target site accessibility.

Evolutionary Conservation of *FGFRL1* 3' UTR Harboring rs4647940

Multiple sequence alignment of orthologous sequences of *FGFRL1* 3' UTR segment encompassing rs4647940 from human, chimpanzee, gorilla, gibbon, orangutan, and rhesus macaque species showed that this SNP corresponds to a highly conserved nucleotide (Fig. 6), which could be under high selective pressures during evolution, and therefore is likely functional.

Predicted miRNAs that Potentially Bind to *FGFRL1* rs4647940

Based on predictions of four *in silico* tools (i.e., MicroSNiPer, MirSNP, RegRNA 2.0, and

TargetScan), 13 miRNAs could target *FGFRL1* rs4647940 (Table 3).

Differential Expressions of Mouse miRNA Orthologs in Bone during Skeletal

Development

Based on miRNA-seq study of a mouse model for age-related osteoporosis (41), i.e., mmu-miR-140-5p, mmu-miR-143-5p, mmu-miR-34c-5p, mmu-miR-106b-3p, mmu-miR-30c-2-3p, mmu-miR-92a-2-5p, and mmu-miR-17-3p, were differentially expressed between 25-m versus 2-m, 8-m versus 2-m, and 25-m versus 8-m time points in bone (Table 4), with their corresponding human orthologs highlighted in Table 3. Two of them, i.e., mmu-miR-34c-5p and mmu-miR-140-5p, not only were significantly differentially expressed across all three comparisons, but also had same directions of fold changes (FCs) (i.e., consistently down-regulated from 2, to 8 and to 25 months). Most prominently, mmu-miR-140-5p had greatest FCs (5.88-, 4-, and 1.47-folds of down-regulation) among these 7 miRNAs, which attained highest statistical significance levels for 25-m versus 2-m ($P\text{-value} = 9.15 \times 10^{-91}$) and 8-m versus 2-m ($P\text{-value} = 9.63 \times 10^{-82}$) comparisons. Because hsa-miR-140-5p is highly conserved during evolution across a wide spectrum of species (Supplementary Material, Fig. S2), such that both mmu-miR-140-5p and dre-miR-140-5p have same sequences as hsa-miR-140-5p, only hsa-miR-140-5p was chosen for experimental validation.

***In vitro* Dual Luciferase Reporter Assay Results**

Human *FGFRL1* gene, which resides in chromosome 4p16.3, consists of six exons. Exon 1 contains 5' UTR followed by a coding sequence for signal peptide (SP). Exons 2, 4, and 5

encode immunoglobulin (Ig)-like C2-type 1, Ig-like C2-type 2, and Ig-like C2-type 3 domains respectively. Exon 6 encodes transmembrane (TM) domain, cytoplasmic tail, and 3' UTR.

Exon-intron structure of *FGFRL1* is highly conserved based on previous phylogenetic analysis (42), and rs4647940 is located in the 3' UTR, which is a part of exon 6 (Fig. 7).

FGFRL1 rs4647940 WT allele (i.e., "C") is complementary with the third position (underlined) of hsa-miR-140-5p 5' seed region (i.e., 5'-CAGUGG-3'), whereas MUT allele (i.e., "G") causes a mismatch. In dual luciferase reporter assay, a negative control (NC) miRNA mimic was co-transfected with an empty vector, or a vector carrying *FGFRL1* 3' UTR WT insert, or a vector carrying *FGFRL1* 3' UTR MUT insert. In human embryonic kidney (HEK) 293 cells, for NC miRNA co-transfection, compared with an empty vector as baseline, a vector carrying either *FGFRL1* 3' UTR WT insert ($-12.15 \pm 4.83\%$, P-value = 0.031) or *FGFRL1* 3' UTR MUT insert ($-18.33 \pm 5.66\%$, P-value = 8.88×10^{-3}) demonstrated significant inhibitions of respective relative luciferase activities, but no statistically significant difference was observed between 3' UTR WT and MUT inserts (P-value = 0.20) (Fig. 8). For hsa-miR-140-5p co-transfection, compared with an empty vector, a vector carrying either *FGFRL1* 3' UTR WT insert ($-45.07 \pm 3.90\%$, P-value = 4.19×10^{-7}) or *FGFRL1* 3' UTR MUT insert ($-48.20 \pm 5.95\%$, P-value = 1.06×10^{-5}) exhibited significant inhibitions of relative luciferase activities. No statistically significant difference was detected between 3' UTR WT and MUT inserts (P-value = 0.58). Nonetheless, relative luciferase activities differed significantly between NC miRNA and hsa-miR-140-5p for both 3' UTR WT insert (P-value = 1.33×10^{-5}) and 3' UTR MUT insert (P-value = 0.0051), indicating that the *FGFRL1* 3' UTR insert bearing rs4647940 is a potential target site for hsa-miR-140-5p.

***In vivo* Zebrafish Microinjection Experiment Results**

Three independent miRNA microinjection experiments were performed, with similar morphological phenotype results obtained. Data from a representative experiment of them were shown in Fig. 9. $N=11$, 14 and 14 zebrafish embryos were respectively included in none-injection control (left panel), NC miRNA-injected (middle panel), and dre-miR-140-5p-injected (right panel) groups. Morphological phenotypes were obtained at two time points — 5 days post-fertilization (dpf) and 7 dpf, respectively. Fig. 9a-f compared zebrafish skeletal morphologies across none-injection control, NC miRNA-injected, and dre-miR-140-5p-injected groups at 5 dpf, whereas Fig. 9g-o compared skeletal morphologies across them at 7 dpf, respectively. At 5 dpf, the body length of dre-miR-140-5p-injected larva appeared shorter (in example shown, 22.61%) compared to either none-injection control, or NC miRNA-injected larva, which had same lengths (Fig. 9a-c). A similar pattern of body length comparisons was observed at 7 dpf (Fig. 9g-i). Further, compared to none-injection control and NC miRNA-injected larvae at 5 dpf (Fig. 9d and j) and 7 dpf (Fig. 9e and k), dre-miR-140-5p-injected larvae at 5 dpf (Fig. 9f) and 7 dpf (Fig. 9l) showed *somewhat reduced* Meckel's cartilage (denoted by “m”) and *almost absent* ceratobranchial cartilages (denoted by “cb1-5”). Significant skeletal morphological differences were detected between none-injection control/NC miRNA-injected and dre-miR-140-5p-injected larvae at 7 dpf (Fig. 9m-o). Florescent images demonstrated that notochord (denoted by “nc”) and parasphenoid (denoted by “ps”) were present in none-injection control and NC miRNA-injected groups (Fig. 9m and n), but were absent in dre-miR-140-5p-injected group (Fig. 9o). Overall, skeletal

malformations were observed in 0/14 (0.00%), 2/14 (14.29%), and 5/11 (45.45%) for none-injection control, NC miRNA-injected, and dre-miR-140-5p-injected groups, respectively. Although the percentage of dre-miR-140-5p-injected group (45.45%) was not statistically different from that of NC miRNA-injected group (14.29%) [P-value (two-sided) = 0.18], the percentage of none-injection group (0.00%) was significantly different from that of dre-miR-140-5p-injected group (45.45%) with a P-value (two-sided) = 0.0087. Further, none-injection control + NC miRNA-injected groups compared with dre-miR-140-5p-injected group gives a significant P-value (two-sided) = 0.012.

DISCUSSION

A traditional GWA meta-analysis approach has been widely applied for discovering novel genetic loci for common human diseases. To date, such an approach has identified a large number of genetic loci underlying disease susceptibilities (43-45). However, in traditional GWA studies, the significantly associated variants are seldom those that play functional roles in phenotypic determination, but are instead in high LD with a causal variant. Consequently, the identification of causal variants is important in understanding molecular mechanisms underlying disease pathogenesis, such that additional well-focused intensive studies (e.g., fine mapping) are required to complement traditional GWA studies to identify disease-causing alleles. Because a functional candidate genomic region association approach focusing exclusively on SNPs with higher prior probabilities for biological functions may increase the type I error rate (i.e., α), the best strategy to differentiate true positives from false positives is to perform replication studies in independent samples. Therefore, focusing exclusively on

those poly-miRTSs, a multi-stage approach, which typically includes a GWA discovery stage followed by *in silico* and *de novo* genotyping replication stages, is a conservative strategy to identify novel functional SNPs located in non-coding 3' UTRs potentially undetected by previous traditional GWA meta-analysis studies due to an overly strict statistical significance threshold. Such a “*hybrid*” approach combines *strengths* of both a *multi-stage GWA meta-analysis approach* and a *hypothesis-driven approach*. Johnson et al. (29) employed a similar multi-stage strategy of the current study for blood pressure and hypertension traits focusing exclusively on 6,683 SNPs located within 60-kb of each of 30 candidate gene regions encoding known anti-hypertensive drug targets in stage I. Two novel SNPs, i.e., *ADRB1* rs1801253 [for systolic blood pressure (SBP) and diastolic blood pressure (DBP)], and *AGT* rs2004776 (for DBP) were identified and replicated, which were missed by their previous traditional GWA scan (i.e., CHARGE Consortium) (46). Another study by Xu et al. (2014) (47) also applied a functional candidate gene association approach for coronary artery disease (CAD) that revealed two novel regulatory SNPs (rs7842 and rs4400266) located respectively in *C3AR1* and *C6* genes to be associated with CAD, which were missed by previous traditional GWA scans.

By interrogating exclusively 41,102 poly-miRTSs collected from PolymiRTS database (48, 49), the probability of detecting functional poly-miRTSs causally linked with BMD traits has significantly increased. A total of 11 stage I-selected poly-miRTSs (corresponding to 10 chromosomal loci) were selected based on (i) statistical significance threshold, (ii) allelic association direction, and (iii) biological significance. In stage II *in silico* replication,

FGFRL1 rs4647940 (P-value = 5.078×10^{-3}) met a relatively stringent statistical significance threshold (i.e., P-value $< 9.09 \times 10^{-3}$) for FN-BMD in gender-combined sample. Because *FGFRL1* rs4647940 is top signal among these stage I-selected 11 poly-miRTSs for FN-BMD in gender-combined sample, in order to avoid missing potentially functional poly-miRTSs for FN-BMD trait, among these 11 stage I-selected poly-miRTSs, we also included stage I's second top signal for FN-BMD in gender-combined sample, i.e., *PRR5* poly-miRTS rs3213550 (P-value: 1.58×10^{-5}), which is a disease-associated miRTSdSNP, although this SNP did not reach stage II significance threshold. In stage III, based on Bonferroni-corrected statistical significance threshold (P-value $< 0.05/2=0.025$) for FN-BMD trait in gender-combined sample, only *FGFRL1* rs4647940 attained statistical significance (Fig. 1). In Zhang et al. (34), 33 stage 1-selected SNPs [i.e., 10 SNPs reaching GWS (i.e., $\alpha = 5.00 \times 10^{-8}$) and 23 SNPs reaching borderline significance (i.e., $\alpha = 1.00 \times 10^{-6}$)] corresponding to 33 chromosomal loci were selected and subjected to stage 2 *in silico* analysis. None of the current study's 11 stage I-selected poly-miRTSs overlap with these 33 stage 1-selected SNPs of previous traditional study. Four chromosomal loci [i.e., 2q33 (*PTH2R*), 4p16.3 [*intergenic* (currently *IDUA*)], 6q25.1 (*C6orf67-ESR1*) and 20q13.33 (*OSBPL2*)] were shared in common, but were represented by totally different SNPs. Of these 33 stage 1-selected chromosomal loci, 13 previously reported and 2 novel loci reached conventional GWS (34). Of them, only chromosome 4p16.3 [*intergenic* (currently *IDUA*)] was commonly shared with the current study, but was represented by a totally different gene, i.e., *FGFRL1*. Estrada et al. (40) performed a traditional multi-stage GWA scan that studied ~ 2.5 million autosomal + chromosome X SNPs in 17 cohorts ($N=32,961$) in stage 1 (GWA discovery). Based on SNP

selection criteria: (i) $P\text{-value} < 5 \times 10^{-6}$ (both unconditional and conditional analysis) for autosomal SNPs and (ii) $P\text{-value} < 5 \times 10^{-5}$ for Chromosome X SNPs, 96 SNPs (87 autosomal SNPs and 9 chromosome X SNPs) corresponding to 83 chromosomal loci were subject to stage 2 *de novo+in silico* replication in 34 cohorts ($N=50,933$). None of the current study's 11 stage I-selected poly-miRTSs overlap with these 96 stage 1-selected SNPs of Estrada et al. (40), but three chromosomal loci [4p16.3 (*IDUA*), 6q25.1 (*C6orf67-ESR1*) and 11q13.1 (*SCYL1*)] were shared in common, which were represented by totally different SNPs, and at 4p16.3 and 11q13.1, were represented by totally different genes. At stage 2 of Estrada et al. (40), 64 [54 chromosomal loci containing 56 gene loci (40)] of these 96 stage 1-selected SNPs attained conventional GWS (i.e., $P < 5 \times 10^{-8}$, stages 1+2-only), 16 (14 chromosomal loci) of which were further replicated in stage 3 for association with fractures ($P < 5 \times 10^{-4}$, stage 3-only) in 50 fracture cohorts ($N=133,460$). Of these 54 BMD-associated chromosomal loci that attained conventional GWS, only 4p16.3 (*IDUA*) was commonly shared with the current study, but was represented by a totally different gene, i.e., *FGFRL1*. None of those 16 BMD- and fracture-associated loci were shared with the current study. Taken together, *FGFRL1* rs4647940 is a novel poly-miRTS for FN-BMD that has been discovered in stage I and subsequently replicated in stages II and III of the current study, respectively. If *not focusing exclusively* on poly-miRTSs in stage I, this *FGFRL1* rs4647940 ($P\text{-value} = 7.67 \times 10^{-6}$ for FN-BMD at stage I) would *not have been discovered at all* — e.g., this potentially functional SNP *did not reach stage I's borderline significance threshold* $\alpha = 1.0 \times 10^{-6}$ in Zhang et al. (34), and therefore did not survive to be further validated in stages 2 and 3. Therefore, by using a more relaxed statistical significance threshold (i.e., 5×10^{-5} , because only

41,102 poly-miRTSs were examined), this SNP was detected in stage I of the current study, and upon replications in subsequent stages II and III, reached GWS ($P\text{-value} = 8.87 \times 10^{-12}$) in stage I+II+III ($N=24,662$). A meta-analysis of rs4647940 conditional on rs3755955 remained suggestively significant ($P\text{-value} = 1.35 \times 10^{-3}$) for FN-BMD in stage I gender-combined sample at $\alpha = 5.00 \times 10^{-3}$, whereas a meta-analysis of rs4647940 conditional on both rs3755955 and rs6827815: was also significant ($P\text{-value} = 1.33 \times 10^{-3}$) for FN-BMD in stage I gender-combined sample.

For *FGFRL1* rs4647940, based on predictions by four *in silico* programs, 13 human miRNAs could potentially bind to this poly-miRTS site (Table 3). Of them, according to miRNA-seq data (41), mouse orthologs of hsa-miR-17-3p, hsa-miR-30c-2-3p, hsa-miR-34c-5p, hsa-miR-92a-2-5p, hsa-miR-106b-3p, hsa-miR-140-5p and hsa-miR-143-5p appear to be *differentially expressed* at different time points during development in a mouse model of age-related osteoporosis (Table 4). Of them, hsa-miR-140-5p appeared to exhibit *greatest magnitudes of differential expressions* among comparisons of three time points (i.e., 2-m, 8m, and 25-m), and *highest levels of statistical significance* for 25-m versus 2-m and 8-m versus 2-m comparisons (Table 4). To experimentally test the potential biological role of *FGFRL1* poly-miRTS rs4647940, both *in vitro* and *in vivo* functional studies were conducted. First, luciferase activity assay results showed that, when co-transfected with hsa-miR-140-5p, reporter construct containing either *FGFRL1* 3' UTR WT insert or *FGFRL1* 3' UTR MUT insert repressed luciferase activity to similar extents (Fig. 8). These experimental findings are concordant with a regulatory role of hsa-miR-140-5p in modulating *FGFRL1* expression by

binding to this 3' UTR segment harboring rs4647940, causing a pronounced inhibition of luciferase activity. As indicated in both Fig. 7 and Supplementary Material, Fig. S2, hsa-miR-140-5p contains a 6-mer 5' seed region (predicted by MicroSNiPer) that is complementary to *FGFRL1* rs4647940 SNP site. Because miRNAs with 6-mer seed regions typically modestly down-regulate their respective mRNA targets (50), these luciferase activity assay results are in agreement with the notion that *FGFRL1* poly-miRTS rs4647940 is located in 5' seed region binding site of has-miR-140-5p. Because an miRNA's 5' seed sequence plays an important role in target recognition and binding, a 3' UTR polymorphism located in an miRNA's 5' seed region binding site, e.g. *FGFRL1* rs4647940, may have a higher probability of functional importance, compared with a 3' UTR polymorphism located in that miRNA's 3' mismatch tolerant region (MTR) binding site.(51) We further tested whether hsa-miR-140-5p plays a significant role in skeletal formation *in vivo*. Nakamura et al. (52) demonstrated that *Mir140*^{-/-} mice had shortened endochondral bones. In another *Mir140*^{-/-} mouse model, a mild skeletal phenotype was observed postnatally, with reduced stature and lower body weight, as well as craniofacial deformities characterized by shorter snout and domed skull (53). In a previous zebrafish model, *mir140* is found expressed in cartilage of pharyngeal arches and in head skeleton (54). Further, Eberhart et al. (2008) (55) observed that dre-miR-140-5p-injected zebrafish exhibited craniofacial skeletal defects. The current study's *in vivo* zebrafish miRNA microinjection experiments gave rise to similar results, demonstrating that dre-miR-140-5p-injected group had a significantly higher percentage of abnormal craniofacial skeletal formation compared with none-injected control + NC miRNA-injected groups.

Fibroblast growth factor (FGF) signaling pathway is pivotal in a variety of developmental processes, including cartilage formation (56) and bone growth (57). *FGFRL1* is *FGFR* gene family's fifth member, and mutations of *FGFR1- FGFR4* cause skeletal disorders (e.g., craniosynostosis syndromes and chondrodysplasias) (58). Interestingly, *FGFRL1* orthologous genes in species ranging from cnidarians to bilaterians are linked with other FGF signaling pathway members within a physical distance < 10 Mb (42). For instance, in sea urchin, *Fgfr1l* is closely linked to *Fgfr1*. Human *FGFRL1* is located in close proximity to *FGFR3* (42). The fact that *FGFRL1* is physically linked to other FGF signaling pathway genes throughout evolution is suggestive of *FGFRL1*'s functional importance in this biological pathway, and likely, also in bone formation: (i) *FGFRL1* is expressed in skeletal tissues shown by Northern blotting and *in situ* hybridization (59); (ii) a depletion of zebrafish *fgfr1la* and *fgfr1lb* results in a craniofacial phenotype (60); (iii) *Fgfr1l*^{-/-} mice exhibited hypoplasia of all skeletal elements, including shortened axial and appendicular skeletons, malformed vertebrae, small pelvic girdle and small rib cage (61); and (iv) in humans, as in zebrafish and mice, *FGFRL1* could be implicated in craniofacial formation during embryogenesis, such that *FGFRL1* deletions or frameshift mutation result in craniofacial malformations (62-64).

The current study's *in vitro* and *in vivo* experimental validation results, combined with findings of previous functional studies of *FGFRL1* and hsa-miR-140-5p as well as clinical genetic studies of *FGFRL1* gene mutations, provided *strong evidence* that *FGFRL1* and hsa-miR-140-5p, which are evolutionarily conserved, play significant biological roles during skeletogenesis. *FGFRL1* rs4647940, attaining conventional GWS for FN-BMD in the current

study, could change hsa-miR-140-5p's 5' seed region binding site located in *FGFRL1*'s 3' UTR, which could then modulate *FGFRL1*'s mRNA expression level that can affect bone formation.

Our study has several limitations. First, the luciferase activity assay's results demonstrated that *FGFRL1* 3' UTR WT and MUT inserts could both bind to hsa-miR-140-5p rather than NC miRNA, but MUT allele did not appear to significantly de-repress luciferase activity in comparison with WT allele. However, rs4647940 may only have a relatively moderate effect on *FGFRL1* mRNA-hsa-miR-140-5p binding, because 5' seed region of hsa-miR-140-5p is a 6-mer. Further, multiple factors could affect results of luciferase activity assay, such as insert length, cell line, and transfection conditions. Besides hsa-miR-140-5p, *FGFRL1* rs4647940 could affect other bone metabolism-related miRNAs' binding sites, e.g., hsa-miR-17-3p and hsa-miR-92a-2-5p (Table 3) predicted by RNAfold. Second, *in vivo* experiment in zebrafish model showed that dre-miR-140-5p microinjection results in a dramatic effect on bone development (Fig. 9), but whether such an effect was mediated by its binding with a target site located on 3' UTR of either *fgfr11a* or *fgfr11b* in zebrafish remains to be elucidated. Nevertheless, results of mouse miRNA-seq (Table 4) and zebrafish microinjection (Fig. 9) experiments unequivocally demonstrated a critical role of miR-140-5p in bone growth. Given that *FGFRL1* rs4647940 is possibly located in a 5' seed region binding site of miR-140-5p based on *in vitro* luciferase activity assay results (Fig. 7), *FGFRL1* rs4647940 is likely a regulatory variant causally linked with BMD.

Taken together, through a combination of a three-stage, poly-miRTS-centric GWA meta-analysis and functional experiments, *FGFRL1* poly-miRTS rs4647940 is significantly associated with FN-BMD trait, attaining conventional GWS. Based on abundant data accumulated from *in vitro* and *in vivo* experimental and clinical genetics studies, *FGFRL1* rs4647940 is likely to play an important role in modulating expressions of *FGFRL1* during skeletogenesis, and further functional characterizations of this SNP in bone metabolism is deserved.

MATERIALS AND METHODS

A flow chart outlining steps of the current study is depicted in Fig. 1. Detailed information on study participants, phenotype measurement and modeling, DNA genotyping, quality control (QC), and genotype imputation for the three-stage GWA meta-analysis is provided in Supplementary Materials and Methods.

Association Analysis

In the current study, only at stage I (7 GWA cohorts), gender-specific (i.e., male- and female-specific) and gender-combined (i.e., male and female) analyses were performed. Nonetheless, only 4 stage I's GWA cohorts (i.e., OOS, KCOS, COS, and FHS) contain males (Table 1), such that male-specific sample size was much smaller than female-specific sample size, giving rise to less statistical power. Therefore, same as in the traditional GWA scan (34), Q-Q plot was generated only for female-specific and gender-combined samples, respectively. At stages II and III, because there were two cohorts at each stage, only gender-combined analyses were performed. Association

tests at each stage are elaborated as follows. In stage I, associations of 41,102 directly-typed or imputed poly-miRTSs with LS-, HIP-, and FN-BMD traits were tested under an additive genetic model for each GWA cohort. Specifically, for five *population-based* samples — OOS, KCOS, COS, WHI-AA, and WHI-HIS, associations were examined by fitting a linear regression model by MACH2QTL (<http://www.sph.umich.edu/csg/abecasis/MACH/download/>), in which an allele dosage was used as a predictor of phenotype. For two family-based samples — FHS and IFS, a mixed linear model was applied that took into consideration the effect of genetic relatedness within each pedigree (65). In stage II, association analyses in RS sample were performed by MACH2QTL implemented by GRIMP (66). Imputation and association analyses in KoGES were performed by IMPUTE v2 (67) and PLINK (68). Detailed statistical methods for association analyses of HIP-, LS-, and FN-BMD traits in AOGC sample were presented previously by Duncan et al. (2011). Briefly, for HIP-BMD, association analysis for imputed SNPs was performed using an additive genetic model including four EIGENSTRAT eigenvectors by MACH2DAT (69), accounting for uncertainties in imputed genotype data by weighting genotypes by their posterior probabilities. For LS- and FN-BMD, Z-transformed residual BMD scores (in g/cm²) were generated for the entire AOGC cohort after adjusting for age, age², weight, and center of BMD measurement. An association test developed by Kung et al. (2010) (70) was applied to account for selections of extreme samples. In stage III, association tests were carried out using PLINK (68) for each study.

Meta-analysis

As described by Zhang et al. (2014) (34), a p-value based meta-analysis was used in METAL

(<http://www.sph.umich.edu/csg/abecasis/metal/>) (71), weighted by square root of sample size.

Cochran's Q statistic and I^2 were computed as measures of between-study heterogeneity. Random-effect meta-analyses were performed for those poly-miRTSs with Q statistic P-value < 0.05 or I^2 value > 50% by applying the “rmeta” package (<http://cran.r-project.org/web/packages/rmeta/index.html>). In stage 1, meta-analysis of a given SNP conditional on one or two other SNPs in LD was also performed by GCTA version 1.20 (<http://www.complextraitgenomics.com/software/gcta/massoc.html>) (72).

Regional Association Plot and Linkage Disequilibrium (LD) r^2 Plot

Regional association plots were generated by applying LocusZoom (<http://csg.sph.umich.edu/locuszoom/>) (73). LD r^2 Plots were generated by Haploview (74, 75) for 58 SNPs at chromosome 4p16.3 for OOS and KCOS cohorts, respectively.

Poly-miRTSs in miRNA Target Sites

The poly-miRTS-*centric* GWA meta-analysis focuses exclusively on 41,102 poly-miRTSs in stage I, in contrast to 5,842,825 SNPs in stage 1 of previous traditional GWA scan (34).

Detailed information on poly-miRTS selection is presented in Supplementary Material, Text S1.

Computational Predictions of RNA Secondary Structures

The miRNA-mRNA hybridization is a two-step process such that an miRNA first binds to a short accessible region of its target mRNA, and then, the target mRNA's secondary structure

unfolds as the miRNA completes its binding to target site (76). The secondary structure of an mRNA can influence its accessibility to miRNA (77). In order to assess potential impacts of WT and MUT alleles on the secondary structure of the 3' UTR of *FGFRL1*, a 121-bp *FGFRL1* 3' UTR segment carrying either WT or MUT allele of rs4647940 were predicted by RNAfold from the Vienna RNA package (<http://rna.tbi.univie.ac.at/cgi-bin/RNAfold.cgi>) (78, 79) based on MFE algorithm with default parameters.

Multiple Sequence Alignment and Sequence Logo

Polymorphisms located at evolutionarily conserved nucleotides are likely to be of greater functional significance than those located at evolutionarily divergent nucleotides. To further bioinformatically assess functional significance for *FGFRL1* rs4647940, cross-species comparisons of orthologous sequences of *FGFRL1* 3' UTR segment encompassing rs4647940 from six species, i.e., human, chimpanzee, gorilla, gibbon, orangutan, and rhesus macaque, was performed by ClustalX version 1.81 (80) with default parameters. A Sequence Logo corresponding to a middle 15-bp DNA segment was generated using WebLogo online program (81).

***In Silico* Predictions of miRNAs that Bind to a Poly-miRTS**

Human miRNAs that could bind to *FGFRL1* rs4647940 were predicted by four online tools:

- (i) MicroSNiPer (<http://cbdb.nimh.nih.gov/microsniper>) (82), (ii) MirSNP (<http://cmbi.bjmu.edu.cn/mirsnp>) (83), (iii) RegRNA 2.0 (<http://regrna2.mbc.nctu.edu.tw/>) (84, 85), and (iv) TargetScan (<http://www.targetscan.org/>) 6.2 (11, 16, 86).

***In Vitro* Dual Luciferase Reporter Assays**

To assess whether *FGFRL1* 3' UTR segment containing either WT or MUT allele of rs4647940 could bind to hsa-miR-140-5p *in vitro*, a pmirGLO dual-luciferase miRNA target expression vector harboring *FGFRL1* 3' UTR WT or MUT inset was constructed, which was subsequently transfected into HEK 293 cells. Details about cloning and transfection, as well as luciferase activity assays are presented in Supplementary Material, Text S1.

***In vivo* Zebrafish Microinjection Experiments**

To assess an *in vivo* role of hsa-miR-140-5p in bone formation, zebrafish microinjection experiments were performed, with each experiment consisting of three groups: (1) a none-injection control group, (2) an NC miRNA microinjection group, and (3) a dre-miR-140-5p microinjection group, respectively. Detailed experimental procedures were described in Supplementary Material, Text S1. These procedures were repeated three times, and microscope image data of morphological phenotypes from a representative experiment at 5 dpf and 7 dpf were obtained from each respective group.

ACKNOWLEDGMENTS

We thank Dr. Karol Estrada and Dr. Fernando Rivadeneira (both from Department of Internal Medicine and Department of Epidemiology, Erasmus Medical Center, Rotterdam, The Netherlands) for their help with analyzing and delivering the Rotterdam Study data, and Tian Hu (Department of Epidemiology, Tulane University School of Public Health and Tropical Medicine) for assistance in generating the meta-analysis figure. We are grateful for Dr. Jesse D. Ziebarth and Dr. Yan Cui (both from University of Tennessee Health Science Center) for helpful comments on application of PolymiRTS Databases. The AOGC thanks the research nurses involved in this study (Ms Barbara Mason and Ms Amanda Horne (Auckland), Ms Linda Bradbury and Ms Kate Lowings (Brisbane), Ms Katherine Kolk and Ms Rumbidzai Tichawangana (Geelong); Ms Helen Steane (Hobart); Ms Jemma Christie (Melbourne); and Ms Janelle Rampellini (Perth). The AOGC also acknowledges gratefully technical support from Ms Kathryn Addison, Ms Marieke-Brugmans, Ms Catherine Cremen, Ms Johanna Hadler and Ms Karena Pryce.

SUPPLEMENTARY MATERIAL

Supplementary Material is available at *HMG* online.

Conflict of interest Statement. None declared.

FUNDING

The study was partially supported by Shanghai Leading Academic Discipline Project (S30501) and startup fund from Shanghai University of Science and Technology. The investigators of this work were also supported by grants from NIH (P50AR055081, R01AG026564, R01AR050496, RC2DE020756, R01AR057049, R03TW008221, and R01GM109068) and the Franklin D. Dickson/Missouri Endowment and the Edward G. Schlieder Endowment.

The Framingham Heart Study (FHS) is conducted and supported by the National Heart, Lung, and Blood Institute (NHLBI) in collaboration with Boston University (Contract Number N01-HC-25195). This manuscript was not prepared in collaboration with investigators of FHS and does not necessarily reflect the opinions or views of FHS, Boston University, or NHLBI.

Funding for SHARe genotyping was provided by NHLBI Contract N02-HL-64278. SHARe

Illumina genotyping was provided under an agreement between Illumina and Boston

University. Funding support for the Framingham Bone Mineral Density datasets was provided by NIH grants R01 AR/AG 41398, R01 AR050066 and R03 AG20321.

Funding support for the Genetic Determinants of Bone Fragility was provided through the

National Institute of Aging (NIA) Division of Geriatrics and Clinical Gerontology. Genetic

Determinants of Bone Fragility is a genome-wide association studies funded as part of the

NIA Division of Geriatrics and Clinical Gerontology. Assistance with phenotype

harmonization and genotype cleaning, as well as with general study coordination, was

provided by the NIA Division of Geriatrics and Clinical Gerontology and the NIA Division of

Aging Biology. Support for the collection of datasets and samples were provided by the

parent grant, Genetic Determinants of Bone Fragility (P01-AG018397). Funding support for

the genotyping which was performed at the Johns Hopkins University Center for Inherited Diseases Research was provided by the NIH NIA.

The Women's Health Initiative (WHI) program is funded by the NHLBI, National Institutes of Health, U.S. Department of Health and Human Services through contracts N01WH22110, 24152, 32100-2, 32105-6, 32108-9, 32111-13, 32115, 32118-32119, 32122, 42107-26, 42129-32, and 44221. This manuscript was not prepared in collaboration with investigators of the WHI, has not been reviewed and/or approved by WHI, and does not necessarily reflect the opinions of the WHI investigators or the NHLBI. WHI Population Architecture Using Genomics and Epidemiology (PAGE) is funded through the NHGRI PAGE network (U01HG004790). Assistance with phenotype harmonization, SNP selection, data cleaning, meta-analyses, data management and dissemination, and general study coordination, was provided by the PAGE Coordinating Center (U01HG004801-01). The datasets used for the analyses described in this manuscript were obtained from the database of Genotypes and Phenotypes (dbGaP) at <http://www.ncbi.nlm.nih.gov/sites/entrez?db=gap> through dbGaP accession phs000200.v6.p2.

This work was supported in part by the Netherlands Organization of Scientific Research NWO Investments (175.010.2005.011 and 911-03-012 to K.E., F.R. and A.G.U.); the Research Institute for Diseases in the Elderly (014-93-015 and RIDE2 to K.E., F.R. and A.G.U.); the Netherlands Genomics Initiative (NGI)/Netherlands Organization for Scientific Research (050-060-810 to K.E., F.R. and A.G.U.); the National Genome Research Institute, Korean Center for Disease Control and Prevention (2001-2003-348- 6111-221, 2004-347-6111-213 and 2005-347-2400-2440-215 to H.J.C., J.Y.L., B.G.H., C.S.S. and N.H.C.); the

Australian Cancer Research Foundation and Rebecca Cooper Foundation (511132 to AOGC) and the National Health and Medical Research Council (Australia) Career Development Award (569807 to E.L.D.). Funding of AOGC was also received from the Australian Cancer Research Foundation and Rebecca Cooper Foundation (Australia). The Rotterdam study is funded by Erasmus Medical Center and Erasmus University, Rotterdam, Netherlands Organization for the Health Research and Development (ZonMw), the Research Institute for Diseases in the Elderly (RIDE), the Ministry of Education, Culture and Science, the Ministry for Health, Welfare and Sports, the European Commission (DG XII) and the Municipality of Rotterdam. T.N. is supported in part by a start-up fund of Tulane University. L.Z. is partially supported by National Natural Science Foundation of China project (31100902). M.A.B. is funded by a National Health and Medical Research Council (Australia) Senior Principal Research Fellowship. Y.-P. W. is funded by the U.S. National Institutes of Health and National Science Foundation. H.-W. D. is partially supported by the Franklin D. Dickson/Missouri Endowment and is supported by the Edward G. Schlieder Endowment.

REFERENCES

1. Kanis, J.A., Melton, L.J., 3rd, Christiansen, C., Johnston, C.C. and Khaltsev, N. (1994) The diagnosis of osteoporosis. *J Bone Miner. Res.*, **9**, 1137-1141.
2. Cardon, L.R., Garner, C., Bennett, S.T., Mackay, I.J., Edwards, R.M., Cornish, J., Hegde, M., Murray, M.A., Reid, I.R. and Cundy, T. (2000) Evidence for a major gene for bone mineral density in idiopathic osteoporotic families. *J Bone Miner. Res.*, **15**, 1132-1137.
3. Howard, G.M., Nguyen, T.V., Harris, M., Kelly, P.J. and Eisman, J.A. (1998) Genetic and environmental contributions to the association between quantitative ultrasound and bone mineral density measurements: a twin study. *J Bone Miner. Res.*, **13**, 1318-1327.
4. Nguyen, T.V., Howard, G.M., Kelly, P.J. and Eisman, J.A. (1998) Bone mass, lean mass, and fat mass: same genes or same environments? *Am. J. Epidemiol.*, **147**, 3-16.
5. Peacock, M., Turner, C.H., Econs, M.J. and Foroud, T. (2002) Genetics of osteoporosis. *Endocr. Rev.*, **23**, 303-326.
6. Yang, T.L., Zhao, L.J., Liu, Y.J., Liu, J.F., Recker, R.R. and Deng, H.W. (2006) Genetic and environmental correlations of bone mineral density at different skeletal sites in females and males. *Calcif. Tissue Int.*, **78**, 212-217.
7. Chang, T.C. and Mendell, J.T. (2007) microRNAs in vertebrate physiology and human disease. *Annu. Rev. Genomics Hum. Genet.*, **8**, 215-239.
8. Gu, S. and Kay, M.A. (2010) How do miRNAs mediate translational repression? *Silence*, **1**, 11.
9. Kozomara, A. and Griffiths-Jones, S. (2014) miRBase: annotating high confidence microRNAs using deep sequencing data. *Nucleic Acids Res.*, **42**, D68-73.
10. Thomas, L.F. and Saetrom, P. (2014) Circular RNAs are depleted of polymorphisms at

microRNA binding sites. *Bioinformatics*, **30**, 2243-2246.

11. Friedman, R.C., Farh, K.K., Burge, C.B. and Bartel, D.P. (2009) Most mammalian mRNAs are conserved targets of microRNAs. *Genome Res.*, **19**, 92-105.
12. Bartel, D.P. (2004) MicroRNAs: genomics, biogenesis, mechanism, and function. *Cell*, **116**, 281-297.
13. Krek, A., Grun, D., Poy, M.N., Wolf, R., Rosenberg, L., Epstein, E.J., MacMenamin, P., da Piedade, I., Gunsalus, K.C., Stoffel, M. *et al.* (2005) Combinatorial microRNA target predictions. *Nat. Genet.*, **37**, 495-500.
14. Doench, J.G. and Sharp, P.A. (2004) Specificity of microRNA target selection in translational repression. *Genes Dev.*, **18**, 504-511.
15. Brennecke, J., Stark, A., Russell, R.B. and Cohen, S.M. (2005) Principles of microRNA-target recognition. *PLoS Biol.*, **3**, e85.
16. Lewis, B.P., Burge, C.B. and Bartel, D.P. (2005) Conserved seed pairing, often flanked by adenosines, indicates that thousands of human genes are microRNA targets. *Cell*, **120**, 15-20.
17. Ameres, S.L., Martinez, J. and Schroeder, R. (2007) Molecular basis for target RNA recognition and cleavage by human RISC. *Cell*, **130**, 101-112.
18. Haley, B. and Zamore, P.D. (2004) Kinetic analysis of the RNAi enzyme complex. *Nat. Struct. Mol. Biol.*, **11**, 599-606.
19. Maragkakis, M., Alexiou, P., Papadopoulos, G.L., Reczko, M., Dalamagas, T., Giannopoulos, G., Goumas, G., Koukis, E., Kourtis, K., Simossis, V.A. *et al.* (2009) Accurate microRNA target prediction correlates with protein repression levels. *BMC Bioinformatics*, **10**, 295.
20. Chi, S.W., Hannon, G.J. and Darnell, R.B. (2012) An alternative mode of microRNA target

recognition. *Nat. Struct. Mol. Biol.*, **19**, 321-327.

21. Haas, U., Sczakiel, G. and Laufer, S.D. (2012) MicroRNA-mediated regulation of gene expression is affected by disease-associated SNPs within the 3'-UTR via altered RNA structure. *RNA Biol.*, **9**, 924-937.
22. Chen, K. and Rajewsky, N. (2006) Natural selection on human microRNA binding sites inferred from SNP data. *Nat. Genet.*, **38**, 1452-1456.
23. Chin, L.J., Ratner, E., Leng, S., Zhai, R., Nallur, S., Babar, I., Muller, R.U., Straka, E., Su, L., Burki, E.A. *et al.* (2008) A SNP in a let-7 microRNA complementary site in the KRAS 3' untranslated region increases non-small cell lung cancer risk. *Cancer Res.*, **68**, 8535-8540.
24. Mishra, P.J., Mishra, P.J., Banerjee, D. and Bertino, J.R. (2008) MiRSNPs or MiR-polymorphisms, new players in microRNA mediated regulation of the cell: Introducing microRNA pharmacogenomics. *Cell Cycle*, **7**, 853-858.
25. Abelson, J.F., Kwan, K.Y., O'Roak, B.J., Baek, D.Y., Stillman, A.A., Morgan, T.M., Mathews, C.A., Pauls, D.L., Rasin, M.R., Gunel, M. *et al.* (2005) Sequence variants in SLITRK1 are associated with Tourette's syndrome. *Science*, **310**, 317-320.
26. Dickson, D.W., Baker, M. and Rademakers, R. (2010) Common variant in GRN is a genetic risk factor for hippocampal sclerosis in the elderly. *Neurodegener. Dis.*, **7**, 170-174.
27. Wang, G., van der Walt, J.M., Mayhew, G., Li, Y.J., Zuchner, S., Scott, W.K., Martin, E.R. and Vance, J.M. (2008) Variation in the miRNA-433 binding site of FGF20 confers risk for Parkinson disease by overexpression of alpha-synuclein. *Am. J. Hum. Genet.*, **82**, 283-289.
28. Landi, D., Gemignani, F., Barale, R. and Landi, S. (2008) A catalog of polymorphisms falling in microRNA-binding regions of cancer genes. *DNA Cell Biol.*, **27**, 35-43.

29. Johnson, A.D., Newton-Cheh, C., Chasman, D.I., Ehret, G.B., Johnson, T., Rose, L., Rice, K., Verwoert, G.C., Launer, L.J., Gudnason, V. *et al.* (2011) Association of hypertension drug target genes with blood pressure and hypertension in 86,588 individuals. *Hypertension*, **57**, 903-910.
30. Welter, D., MacArthur, J., Morales, J., Burdett, T., Hall, P., Junkins, H., Klemm, A., Flicek, P., Manolio, T., Hindorff, L. *et al.* (2014) The NHGRI GWAS Catalog, a curated resource of SNP-trait associations. *Nucleic Acids Res.*, **42**, D1001-1006.
31. Kumar, V., Westra, H.J., Karjalainen, J., Zhernakova, D.V., Esko, T., Hrdlickova, B., Almeida, R., Zhernakova, A., Reinmaa, E., Vosa, U. *et al.* (2013) Human disease-associated genetic variation impacts large intergenic non-coding RNA expression. *PLoS Genet.*, **9**, e1003201.
32. Chen, K., Song, F., Calin, G.A., Wei, Q., Hao, X. and Zhang, W. (2008) Polymorphisms in microRNA targets: a gold mine for molecular epidemiology. *Carcinogenesis*, **29**, 1306-1311.
33. Sethupathy, P. and Collins, F.S. (2008) MicroRNA target site polymorphisms and human disease. *Trends in genetics : Trends. Genet.*, **24**, 489-497.
34. Zhang, L., Choi, H.J., Estrada, K., Leo, P.J., Li, J., Pei, Y.F., Zhang, Y., Lin, Y., Shen, H., Liu, Y.Z. *et al.* (2014) Multistage genome-wide association meta-analyses identified two new loci for bone mineral density. *Hum. Mol. Genet.*, **23**, 1923-1933.
35. Bruno, A.E., Li, L., Kalabus, J.L., Pan, Y., Yu, A. and Hu, Z. (2012) miRdSNP: a database of disease-associated SNPs and microRNA target sites on 3'UTRs of human genes. *BMC Genomics*, **13**, 44.
36. Xian, L., Wu, X., Pang, L., Lou, M., Rosen, C.J., Qiu, T., Crane, J., Frassica, F., Zhang, L., Rodriguez, J.P. *et al.* (2012) Matrix IGF-1 maintains bone mass by activation of mTOR in mesenchymal stem cells. *Nat. Med.*, **18**, 1095-1101.

37. Long, F. (2012) Building strong bones: molecular regulation of the osteoblast lineage. *Nat. Rev. Mol. Cell Biol.*, **13**, 27-38.
38. Fulzele, K., Riddle, R.C., DiGirolamo, D.J., Cao, X., Wan, C., Chen, D., Faugere, M.C., Aja, S., Hussain, M.A., Bruning, J.C. *et al.* (2010) Insulin receptor signaling in osteoblasts regulates postnatal bone acquisition and body composition. *Cell*, **142**, 309-319.
39. Woo, S.Y., Kim, D.H., Jun, C.B., Kim, Y.M., Haar, E.V., Lee, S.I., Hegg, J.W., Bandhakavi, S., Griffin, T.J. and Kim, D.H. (2007) PRR5, a novel component of mTOR complex 2, regulates platelet-derived growth factor receptor beta expression and signaling. *J. Biol. Chem.*, **282**, 25604-25612.
40. Estrada, K., Styrkarsdottir, U., Evangelou, E., Hsu, Y.H., Duncan, E.L., Ntzani, E.E., Oei, L., Albagha, O.M., Amin, N., Kemp, J.P. *et al.* (2012) Genome-wide meta-analysis identifies 56 bone mineral density loci and reveals 14 loci associated with risk of fracture. *Nat. Genet.*, **44**, 491-501.
41. He, X., Zhang, W., Liao, L., Fu, X., Yu, Q. and Jin, Y. (2013) Identification and characterization of microRNAs by high through-put sequencing in mesenchymal stem cells and bone tissue from mice of age-related osteoporosis. *PLoS One*, **8**, e71895.
42. Bertrand, S., Somorjai, I., Garcia-Fernandez, J., Lamonerie, T. and Escriva, H. (2009) FGFRL1 is a neglected putative actor of the FGF signalling pathway present in all major metazoan phyla. *BMC Evol. Biol.*, **9**, 226.
43. Evangelou, E. and Ioannidis, J.P. (2013) Meta-analysis methods for genome-wide association studies and beyond. *Nat. Rev. Genet.*, **14**, 379-389.
44. Panagiotou, O.A., Willer, C.J., Hirschhorn, J.N. and Ioannidis, J.P. (2013) The power of meta-analysis in genome-wide association studies. *Annu. Rev. Genomics Hum. Genet.*, **14**, 441-465.
45. Zeggini, E. and Ioannidis, J.P. (2009) Meta-analysis in genome-wide association studies.

Pharmacogenomics, **10**, 191-201.

46. Levy, D., Ehret, G.B., Rice, K., Verwoert, G.C., Launer, L.J., Dehghan, A., Glazer, N.L., Morrison, A.C., Johnson, A.D., Aspelund, T. *et al.* (2009) Genome-wide association study of blood pressure and hypertension. *Nat. Genet.*, **41**, 677-687.
47. Xu, C., Yang, Q., Xiong, H., Wang, L., Cai, J., Wang, F., Li, S., Chen, J., Wang, C., Wang, D. *et al.* (2014) Candidate pathway-based genome-wide association studies identify novel associations of genomic variants in the complement system associated with coronary artery disease. *Circ. Cardiovasc. Genet.*, **7**, 887-894.
48. Bao, L., Zhou, M., Wu, L., Lu, L., Goldowitz, D., Williams, R.W. and Cui, Y. (2007) PolymiRTS Database: linking polymorphisms in microRNA target sites with complex traits. *Nucleic Acids Res.*, **35**, D51-54.
49. Ziebarth, J.D., Bhattacharya, A., Chen, A. and Cui, Y. (2012) PolymiRTS Database 2.0: linking polymorphisms in microRNA target sites with human diseases and complex traits. *Nucleic Acids Res.*, **40**, D216-221.
50. Witkos, T.M., Koscianska, E. and Krzyzosiak, W.J. (2011) Practical Aspects of microRNA Target Prediction. *Curr. Mol. Med.*, **11**, 93-109.
51. Mishra, P.J. and Bertino, J.R. (2009) MicroRNA polymorphisms: the future of pharmacogenomics, molecular epidemiology and individualized medicine. *Pharmacogenomics*, **10**, 399-416.
52. Nakamura, Y., Inloes, J.B., Katagiri, T. and Kobayashi, T. (2011) Chondrocyte-specific microRNA-140 regulates endochondral bone development and targets Dnpep to modulate bone morphogenetic protein signaling. *Mol. Cell Biol.*, **31**, 3019-3028.

53. Miyaki, S., Sato, T., Inoue, A., Otsuki, S., Ito, Y., Yokoyama, S., Kato, Y., Takemoto, F., Nakasa, T., Yamashita, S. *et al. Genes Dev.*, **24**, 1173-1185.
54. Wienholds, E., Kloosterman, W.P., Miska, E., Alvarez-Saavedra, E., Berezikov, E., de Bruijn, E., Horvitz, H.R., Kauppinen, S. and Plasterk, R.H. (2005) MicroRNA expression in zebrafish embryonic development. *Science*, **309**, 310-311.
55. Eberhart, J.K., He, X., Swartz, M.E., Yan, Y.L., Song, H., Boling, T.C., Kunerth, A.K., Walker, M.B., Kimmel, C.B. and Postlethwait, J.H. (2008) MicroRNA Mirn140 modulates Pdgf signaling during palatogenesis. *Nat.Genet.*, **40**, 290-298.
56. Walshe, J. and Mason, I. (2003) Fgf signalling is required for formation of cartilage in the head. *Dev. Biol.*, **264**, 522-536.
57. Kronenberg, H.M. (2003) Developmental regulation of the growth plate. *Nature*, **423**, 332-336.
58. Trueb, B. (2011) Biology of FGFR1, the fifth fibroblast growth factor receptor. *Cell Mol. Life Sci.*, **68**, 951-964.
59. Trueb, B., Zhuang, L., Taeschler, S. and Wiedemann, M. (2003) Characterization of FGFR1, a novel fibroblast growth factor (FGF) receptor preferentially expressed in skeletal tissues. *J. Biol. Chem.*, **278**, 33857-33865.
60. Hall, C., Flores, M.V., Murison, G., Crosier, K. and Crosier, P. (2006) An essential role for zebrafish Fgfr1 during gill cartilage development. *Mech. Dev.*, **123**, 925-940.
61. Catela, C., Bilbao-Cortes, D., Slonimsky, E., Kratsios, P., Rosenthal, N. and Te Welscher, P. (2009) Multiple congenital malformations of Wolf-Hirschhorn syndrome are recapitulated in Fgfr1 null mice. *Dis. Model Mech.*, **2**, 283-294.
62. Engbers, H., van der Smagt, J.J., van 't Slot, R., Vermeesch, J.R., Hochstenbach, R. and Poot,

- M. (2009) Wolf-Hirschhorn syndrome facial dysmorphic features in a patient with a terminal 4p16.3 deletion telomeric to the WHSCR and WHSCR 2 regions. *Eur. J. Hum. Genet.*, **17**, 129-132.
63. Rieckmann, T., Zhuang, L., Fluck, C.E. and Trueb, B. (2009) Characterization of the first FGFR1 mutation identified in a craniosynostosis patient. *Biochim. Biophys. Acta.*, **1792**, 112-121.
64. Matoso, E., Ramos, F., Ferrao, J., Pires, L.M., Mascarenhas, A., Melo, J.B. and Carreira, I.M. (2014) Interstitial 287 kb deletion of 4p16.3 including FGFR1 gene associated with language impairment and overgrowth. *Mol. Cytogenet.*, **7**, 87.
65. Zhang, L., Li, J., Pei, Y.F., Liu, Y. and Deng, H.W. (2009) Tests of association for quantitative traits in nuclear families using principal components to correct for population stratification. *Ann. Hum. Genet.*, **73**, 601-613.
66. Estrada, K., Abuseiris, A., Grosveld, F.G., Uitterlinden, A.G., Knoch, T.A. and Rivadeneira, F. (2009) GRIMP: a web- and grid-based tool for high-speed analysis of large-scale genome-wide association using imputed data. *Bioinformatics*, **25**, 2750-2752.
67. Howie, B.N., Donnelly, P. and Marchini, J. (2009) A flexible and accurate genotype imputation method for the next generation of genome-wide association studies. *PLoS Genet.*, **5**, e1000529.
68. Purcell, S., Neale, B., Todd-Brown, K., Thomas, L., Ferreira, M.A., Bender, D., Maller, J., Sklar, P., de Bakker, P.I., Daly, M.J. *et al.* (2007) PLINK: a tool set for whole-genome association and population-based linkage analyses. *Am. J. Hum. Genet.*, **81**, 559-575.
69. Li, Y., Willer, C., Sanna, S. and Abecasis, G. (2009) Genotype imputation. *Annu. Rev. Genomics Hum. Genet.*, **10**, 387-406.
70. Kung, A.W., Xiao, S.M., Cherny, S., Li, G.H., Gao, Y., Tso, G., Lau, K.S., Luk, K.D., Liu, J.M.,

- Cui, B. *et al.* (2010) Association of JAG1 with bone mineral density and osteoporotic fractures: a genome-wide association study and follow-up replication studies. *Am. J. Hum. Genet.*, **86**, 229-239.
71. Willer, C.J., Li, Y. and Abecasis, G.R. (2010) METAL: fast and efficient meta-analysis of genomewide association scans. *Bioinformatics*, **26**, 2190-2191.
72. Yang, J., Lee, S.H., Goddard, M.E. and Visscher, P.M. (2011) GCTA: a tool for genome-wide complex trait analysis. *Am. J. Hum. Genet.*, **88**, 76-82.
73. Pruim, R.J., Welch, R.P., Sanna, S., Teslovich, T.M., Chines, P.S., Gliedt, T.P., Boehnke, M., Abecasis, G.R. and Willer, C.J. (2010) LocusZoom: regional visualization of genome-wide association scan results. *Bioinformatics*, **26**, 2336-2337.
74. Barrett, J.C., Fry, B., Maller, J. and Daly, M.J. (2005) Haploview: analysis and visualization of LD and haplotype maps. *Bioinformatics*, **21**, 263-265.
75. Barrett, J.C. (2009) Haploview: Visualization and analysis of SNP genotype data. *Cold Spring Harb. Protoc.*, pdb.ip71.
76. Long, D., Lee, R., Williams, P., Chan, C.Y., Ambros, V. and Ding, Y. (2007) Potent effect of target structure on microRNA function. *Nat. Struct. Mol. Biol.*, **14**, 287-294.
77. Mahen, E.M., Watson, P.Y., Cottrell, J.W. and Fedor, M.J. (2010) mRNA secondary structures fold sequentially but exchange rapidly in vivo. *PLoS Biol.*, **8**, e1000307.
78. Gruber, A.R., Lorenz, R., Bernhart, S.H., Neubock, R. and Hofacker, I.L. (2008) The Vienna RNA websuite. *Nucleic Acids Res.*, **36**, W70-74.
79. Hofacker, I.L. (2003) Vienna RNA secondary structure server. *Nucleic Acids Res.*, **31**, 3429-3431.
80. Jeanmougin, F., Thompson, J.D., Gouy, M., Higgins, D.G. and Gibson, T.J. (1998) Multiple

sequence alignment with Clustal X. *Trends Biochem. Sci.*, **23**, 403-405.

81. Crooks, G.E., Hon, G., Chandonia, J.M. and Brenner, S.E. (2004) WebLogo: a sequence logo generator. *Genome Res.*, **14**, 1188-1190.
82. Barenboim, M., Zoltick, B.J., Guo, Y. and Weinberger, D.R. (2010) MicroSNiPer: a web tool for prediction of SNP effects on putative microRNA targets. *Hum. Mutat.*, **31**, 1223-1232.
83. Liu, C., Zhang, F., Li, T., Lu, M., Wang, L., Yue, W. and Zhang, D. (2012) MirSNP, a database of polymorphisms altering miRNA target sites, identifies miRNA-related SNPs in GWAS SNPs and eQTLs. *BMC Genomics*, **13**, 661.
84. Huang, H.Y., Chien, C.H., Jen, K.H. and Huang, H.D. (2006) RegRNA: an integrated web server for identifying regulatory RNA motifs and elements. *Nucleic Acids Res.*, **34**, W429-434.
85. Chang, T.H., Huang, H.Y., Hsu, J.B., Weng, S.L., Horng, J.T. and Huang, H.D. (2013) An enhanced computational platform for investigating the roles of regulatory RNA and for identifying functional RNA motifs. *BMC Bioinformatics*, **14 Suppl 2**, S4.
86. Grimson, A., Farh, K.K., Johnston, W.K., Garrett-Engele, P., Lim, L.P. and Bartel, D.P. (2007) MicroRNA targeting specificity in mammals: determinants beyond seed pairing. *Mol. Cell*, **27**, 91-105.

FIGURE LEGENDS

Figure 1. A flow chart of the poly-miRTS-centric three-stage GWA meta-analysis and experimental validation. Abbreviations: GWA, genome-wide association; SNP, single nucleotide polymorphism; DB, database; poly-miRTSs, polymorphisms in microRNAs Target Sites; study name abbreviations are shown in footnote of Table 1

Figure 2. A forest plot of *FGFRL1* rs4647940 for FN-BMD trait for stage I+II+III for gender-combined (i.e., Male and Female) Cohort. Abbreviations: BMD, bone mineral density; FN, Femoral Neck

Figure 3. Regional association plots for chromosome 4p16.3 loci *FGFRL1* rs4647940, *IDUA* rs6827815 and *IDUA* rs3755955 for FN-BMD trait (based on hg19/1000 Genomes Mar 2012 EUR). (A) The region encompassing rs4647940 with ± 100 -kb flanking regions, and (B) a zoom-in view of the center region [i.e., the dashed rectangle in (A)], encompassing rs4647940 with ± 27 -kb regions. Abbreviations: BMD, bone mineral density; EUR, European; FN, Femoral Neck

Figure 4. The physical locations and linkage disequilibrium pairwise r^2 plot generated by Haploview (74, 75) for the 80.744-kb human *FGFRL1* region (total 58 SNPs) encompassing *FGFRL1* rs4647940 (current study), rs6827815 (Zhang et al. (34)) and rs3755955 (Estrada et al. (40)) for (A) OOS and (B) KCOS, respectively. Haplotype blocks 1 and 2 are shown by dashed lines. Abbreviations: OOS, Omaha Osteoporosis Study; KCOS, Kansas-City Osteoporosis Study; SNP, single nucleotide polymorphism

Figure 5. Predicted secondary structure of *FGFRL1* 3' UTR 121-bp mRNA sequence carrying either (A) rs4647940-C allele or (B) rs4647940-G allele by RNAfold. Abbreviations:

MFE, minimum free energy; UTR, untranslated region

Figure 6. Cross-species comparison of DNA sequences of *FGFRL1* 3' UTR encompassing rs4647940 in human (GenBank accession number NM_001004356.2), chimpanzee (GenBank accession number AC194569.3), gibbon (GenBank accession number NW_003501383.2), gorilla (GenBank accession number NW_004002168.1), orangutan (GenBank accession number NW_002878038.1), and rhesus macaque (GenBank accession number NW_001111081.1). A 15-bp consensus motif surrounding *FGFRL1* rs4647940 is represented by a WebLogo. The box (a 6-bp sequence) denotes a 5' seed region binding site for hsa-miR-140-5p, which includes *FGFRL1* rs4647940 (i.e., at fourth position). Multiple DNA sequence alignment was performed by ClustalX version 1.81. The asterisks denote nucleotides conserved across all the species that were compared

Figure 7. *FGFRL1* gene structure, rs4647940 physical location, and the potential binding of *FGFRL1* mRNA with hsa-miR-140-5p. Abbreviations: aa, amino acid; bp, base pair; Acc #, Accession Number; Ig, immunoglobulin; SP, signal peptide; TM, transmembrane; UTR, untranslated region; WT, wild-type; MUT, mutant. “|” denotes perfect match; “:” denotes G:U wobble

Figure 8. Dual luciferase report assay results for *FGFRL1* rs4647940. The relative luciferase activities for six different conditions (3 reporter constructs: Empty/WT/MUT vectors, 2 miRNA types: NC miRNA/hsa-miR-140-5p miRNA). On the y-axis, relative luciferase activity (in percentage), was computed as the ratio of firefly luciferase activity to Renilla luciferase activity is given. On the x-axis, different transfection groups are shown. Data are presented as mean \pm SEM from six independent replicates. Abbreviations: miRNA,

microRNA; MUT, mutant; NC, negative control; SEM, standard error of the mean

Figure 9. Craniofacial and overall morphological phenotypes of zebrafish larvae in microRNA microinjection experiments. Left, middle and right panels depict images corresponding to None-injection Control, NC miRNA-injected, and dre-miR-140-5p-injected groups at 5 dpf and 7 dpf larval stages, respectively. The RNA sequence of dre-miR-140-5p is exactly the same as that of hsa-miR-140-5p, indicating cross-species conservation (Supplementary Fig. S1). Three independent experiments comparing None-injection Control, NC miRNA-injected, and dre-miR-140-5p-injected groups were performed, and consistent morphological phenotypes were obtained for each of these three groups across these experiments. Images presented are from one representative experiment. Abbreviations: NC, Negative Control; dpf, days post-fertilization

Table 1. Basic Genotype Information and Phenotype Characteristics of the Study Cohorts at Stages I, II and III*

Sample	N	Population	# Genotyped SNPs	# Imputed SNPs	Female (%)	Age (yrs)	LS-BMD (g/cm ²)	HIP-BMD (g/cm ²)	FN-BMD (g/cm ²)	Bone densitometer
Stage I**	(GWA meta-analysis)									
OOS	987	Caucasian	407,634	6,427,198	49.6	50.3(18.3)	1.03(0.16)	0.97(0.16)	0.81(0.14)	Hologic QDR 4500W
KCOS	2,250	Caucasian	743,768	7,085,256	75.9	51.4(13.8)	1.02(0.16)	0.97(0.17)	0.80(0.15)	Hologic QDR 4500W
COS	1,547	Han Chinese	725,883	5,823,600	50.7	34.8(13.4)	0.95(0.13)	0.92(0.13)	0.81(0.13)	Hologic QDR 4500W
FHS	3,747	Caucasian	405,948	6,456,277	57.3	60.3(10.7)	1.22(0.23)	0.95(0.17)	0.89(0.16)	Lunar DPX-L
IFS	1,488	Caucasian	543,932	7,202,569	100.0	32.7(7.2)	---	---	---	Lunar DPX-L
WHI-AA	712	African American	799,328	11,862,114	100.0	60.9(6.9)	1.05(0.17)	0.95(0.15)	0.83(0.14)	Hologic QDR-2000
WHI-HIS	409	Hispanic	647,362	6,916,926	100.0	60.7(7.2)	0.97(0.16)	0.86(0.13)	0.73(0.12)	Hologic QDR-2000
Total	11,140									
Stage II***	(in silico replication)									
RS	4,904	Caucasian	512,349	6,986,425	57.0	69.4(9.0)	1.09(0.18)	NA	0.86(0.13)	Lunar DPX-L
AOGC	1,955	Caucasian	Region-wise	Region-wise	100.0	69.6(8.6)	1.08(0.26)	0.89(0.25)	0.79(0.21)	Multiple [§]
Total	6,859									
Stage III	(de novo genotyping replication)									
KCOSR	3,923	Caucasian	3	0	57.6	46.8(14.5)	1.03(0.15)	0.96(0.15)	0.80(0.14)	Hologic QDR
COSR	2,740	Han Chinese	3	0	57.7	32.3(14.4)	0.93(0.12)	0.91(0.13)	0.80(0.13)	Hologic QDR 4500W
Total	6,663									

*Adapted from Supplementary Table 1 of Zhang et al. (2014) (34). Although KoGES was included in stage 2 (*in silico* replication) of Zhang et al. (2014) (34), because none of the Korean Genome Epidemiology Study (KoGES) results were included in the *in silico* replication of stage I-selected poly-miRTSs, the stage II (*in silico* replication) of the current study only included RS and AOGC, but not KoGES. Data were presented as mean (SD). N denotes sample size for each study cohort. Abbreviations: OOS, Omaha Osteoporosis Study; KCOS, Kansas-City Osteoporosis Study; COS, China Osteoporosis Study; FHS, Framingham Heart Study; IFS, Indiana Fragility Study; WHI-AA, Women's Health Initiative African American sample; WHI-HIS, Women's Health Initiative Hispanic sample. RS, Rotterdam Study; AOGC, Australian Osteoporosis Genetics Consortium; KCOSR, KCOS Replication; COSR, COS Replication. SNP, single nucleotide polymorphism; poly-miRTS, polymorphism in microRNAs Target Sites; BMD, bone-mineral density; LS, lumbar spine; HIP, total hip; FN, femoral neck. "---", not available. λ_{GC} ranges from 0.99 to 1.06 (34).

**As indicated in Zhang et al. (34), 5842,825 common SNPs (either genotyped or imputed) were shared across the seven stage I Genome Wide-Association studies and only those 41,102 poly-miRTSs were included in stage I.

***As indicated in Zhang et al. (34), for AOGC study, genotype imputations were only performed for specific regions, and only 11 stage I-selected poly-miRTSs were included in stage II of the current study.

§Either Hologic QDR or Lunar DPX-L series was used to measure BMD.

Table 2. GWA Meta-analysis Results for *FGFRL1* and *PRR5* Poly-miRTSs*

Poly-miRTS			Stage I			Stage II			Stage III			Stage I+II+III
dbSNP ID	Locus	Gene	Phenotype	Analysis	P-value	Phenotype	Analysis	P-value	Phenotype	Analysis	P-value	P-value
rs3127592	6q25.3	<i>SLC22A2</i>	HIP-BMD	Combined	3.24×10 ⁻⁶	FN-BMD	Combined	0.5034	---	---	---	---
rs3127593	6q25.3	<i>SLC22A2</i>	HIP-BMD	Combined	6.59×10 ⁻⁶	FN-BMD	Combined	0.4638	---	---	---	---
rs4647940	4p16.3	<i>FGFRL1</i>	FN-BMD	Combined	7.67×10⁻⁶	FN-BMD**	Combined	5.078×10⁻³	FN-BMD**	Combined	7.55×10⁻⁶	8.87×10⁻¹²
rs1599795	3q13.33	<i>CD80</i>	HIP-BMD	Combined	1.32×10 ⁻⁵	FN-BMD	Combined	0.3689	---	---	---	---
rs9479085	6q25.1	<i>C6orf97</i>	LS-BMD	Combined	1.47×10 ⁻⁵	LS-BMD**	Combined	9.202×10 ⁻³	---	---	---	---
rs3213550	22q13.31	<i>PRR5</i>	FN-BMD	Combined	1.58×10 ⁻⁵	FN-BMD**	Combined	0.3138	FN-BMD	Combined	0.08208	1.17×10 ⁻⁵
rs1057392	2q34	<i>PTH2R</i>	HIP-BMD	Combined	2.60×10 ⁻⁵	FN-BMD	Combined	0.3167	---	---	---	---
rs10739677	9q33.3	<i>FAM125B</i>	HIP-BMD	Female	2.67×10 ⁻⁵	FN-BMD	Combined	0.4262	---	---	---	---
rs17547201	17q12	<i>AMAC1</i>	HIP-BMD	Female	2.79×10 ⁻⁵	FN-BMD	Combined	0.4009	---	---	---	---
rs11581122	1p12	<i>FAM46C</i>	HIP-BMD	Combined	4.47×10 ⁻⁵	FN-BMD	Combined	0.6717	---	---	---	---
rs523200	11q13.1	<i>SFI</i>	FN-BMD	Combined	4.76×10 ⁻⁵	FN-BMD**	Combined	0.1879	---	---	---	---

*Abbreviations: BMD, bone mineral density; FN, femoral neck; HIP, total hip; LS, lumbar spine; poly-miRTS, polymorphism in microRNAs Target Sites, SNP, single nucleotide polymorphism. Combined refers to male and female. Genome-wide significance (GWS) is defined as $\alpha = 5.00 \times 10^{-8}$ in the previous traditional study (34) and 5.21×10^{-6} in the current study, respectively. P-values attaining the GWS level are highlighted in bold font. Shaded regions were matched regions between these two studies, although different SNPs were identified. The SNP reaching GWS for stage I+II+III (i.e., P-value < 5.21×10^{-6}) was highlighted in bold font.

**Data were available for two cohorts in each respective stage of stages II and III. Otherwise, data were available for only one cohort in each respective stage of stages II and III.

Table 3. Putative Human miRNAs that Bind to *FGFRL1* Poly-miRTS rs4647940

miR-Name	# Programs	MicroSNiPer	MirSNP Score	RegRNA2.0 Score	TargetScan Context Score Percentile
<i>hsa-miR-17-3p</i>	1	Seed length: 7 (Yes)	--- (No)	<150 (No)	--- (No)
<i>hsa-miR-30c-2-3p</i>	1	Seed length: 7 (Yes)	--- (No)	<150 (No)	--- (No)
<i>hsa-miR-34c-5p</i>	1	Seed length: 6 (Yes)	--- (No)	<150 (No)	--- (No)
<i>hsa-miR-92a-2-5p</i>	1	Seed length: 8 (Yes)	--- (No)	<150 (No)	--- (No)
<i>hsa-miR-106b-3p</i>	1	Seed length: 6 (Yes)	--- (No)	<150 (No)	--- (No)
<i>hsa-miR-140-5p</i>	1	Seed length: 6 (Yes)	--- (No)	<150 (No)	--- (No)
<i>hsa-miR-143-5p</i>	1	Seed length: 6 (Yes)	--- (No)	<150 (No)	--- (No)
hsa-miR-4667-5p	2	Seed length: 8 (Yes)	144.00 (Yes)	<150 (No)	--- (No)
hsa-miR-4700-5p	2	Seed length: 11 (Yes)	161.00 (Yes)	<150 (No)	--- (No)
hsa-miR-4723-5p	2	Seed length: --- (No)	144.00 (Yes)	<150 (No)	77 (Yes)
hsa-miR-5698	2	Seed length: --- (No)	162.00 (Yes)	≥150 (Yes)	--- (No)
hsa-miR-3175	3	Seed length: --- (No)	159.00 (Yes)	≥150 (Yes)	86 (Yes)
hsa-miR-491-5p	4	Seed length: 8 (Yes)	148.00 (Yes)	≥150 (Yes)	76 (Yes)

*Abbreviations: GWA, genome-wide association; poly-miRTS, polymorphism in microRNAs Target Sites; “# Programs”, total number of programs that gave the prediction, denoted by “Yes” in parentheses (otherwise, “No” is shown in parentheses); “---“, not available. Seven human miRNAs that correspond to mouse miRNAs significantly differentially expressed in bone between different time points (He et al., 2013(41)) were *in italic font*, which includes has-miR-140-5p (in bold font). The miRNAs were first sorted by the “# Programs” (lowest to highest), and then sorted by miR number (smallest to largest).

Table 4. Mouse miRNAs that Show Differential Expressions in Bone Among Three Time Points Determined by miRNA-Seq

miR-Name	25-m vs. 2-m		8-m vs. 2-m		25-m vs. 8-m	
	FC	P-value	FC	P-value	FC	P-value
<i>mmu-miR-140-5p</i>	<i>0.17</i>	<i>9.15×10^{-91}</i>	<i>0.25</i>	<i>9.63×10^{-82}</i>	<i>0.68</i>	<i>1.79×10^{-3}</i>
<i>mmu-miR-143-5p</i>	<i>0.45</i>	<i>1.91×10^{-27}</i>	<i>0.34</i>	<i>1.22×10^{-51}</i>	<i>1.34</i>	<i>1.90×10^{-3}</i>
<i>mmu-miR-34c-5p</i>	<i>0.47</i>	<i>7.33×10^{-24}</i>	<i>0.72</i>	<i>8.95×10^{-8}</i>	<i>0.66</i>	<i>1.85×10^{-7}</i>
mmu-miR-106b-3p	1.34	1.10×10^{-4}	1.00	0.96	1.33	1.43×10^{-4}
mmu-miR-30c-2-3p	0.91	0.048	0.88	2.80×10^{-3}	1.04	0.44
mmu-miR-92a-2-5p	0.66	0.1134	1.45	0.061	0.45	1.11×10^{-3}
mmu-miR-17-3p	0.91	0.17	1.90	2.90×10^{-32}	0.47	1.20×10^{-33}

*Abbreviations: 2-m, 2-month; 8-m, 8-month; 25-m, 25-month; FC, fold change. Data were obtained from He et al., 2013 (41). Three mouse miRNAs with significant differences (i.e., P-value < 0.05/3 = 0.0167) of their expressions across three time points (i.e., 2-m, 8-m, and 25-m) were shown in *italic font*, which includes -miR-140-5p (in bold font). The miRNAs were sorted by their levels of statistical significance for 25-m vs. 2-m comparison (highest to lowest).

Figure 1

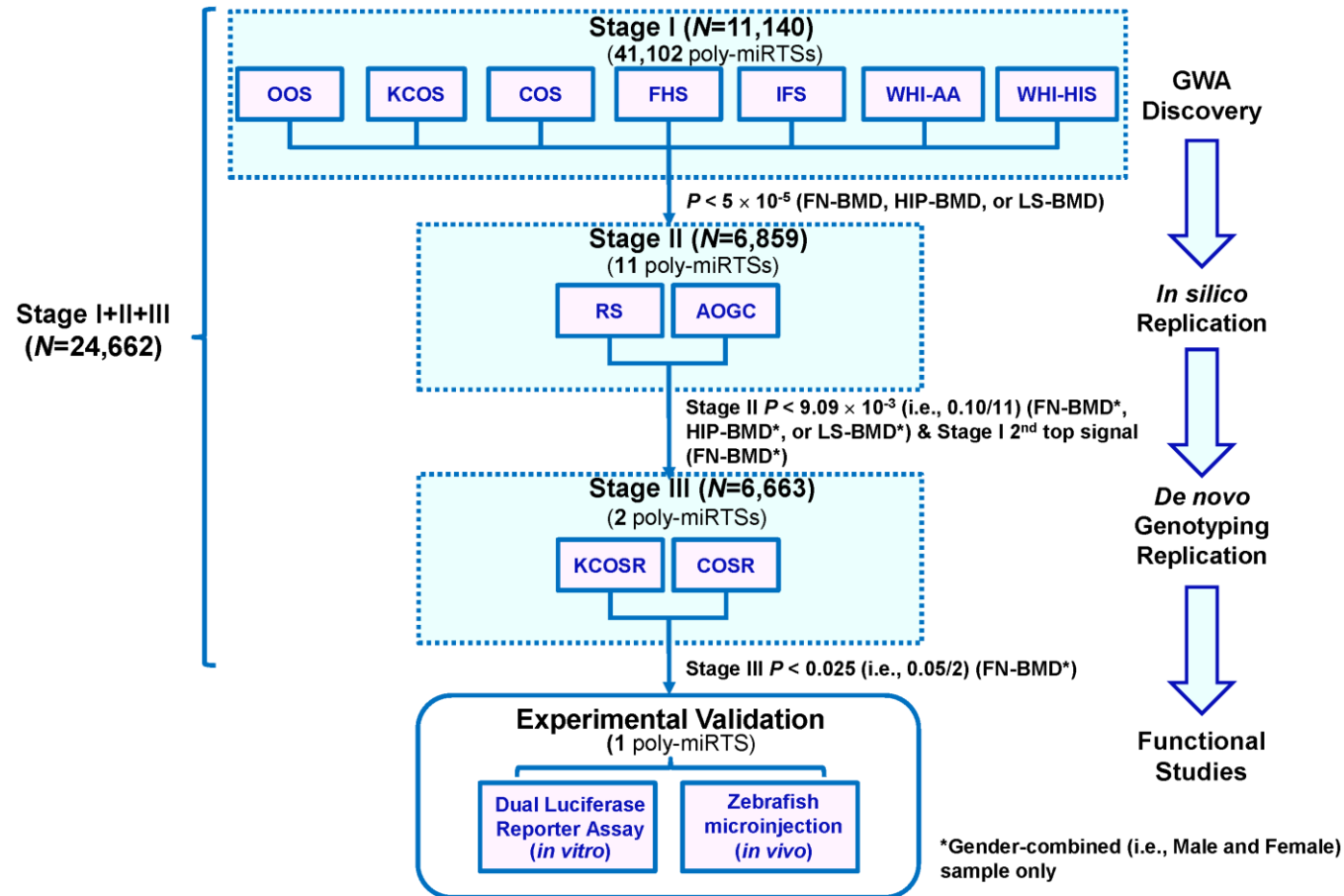


Figure 2
Forest Plot of *FGFRL1* rs4647940 for FN-BMD

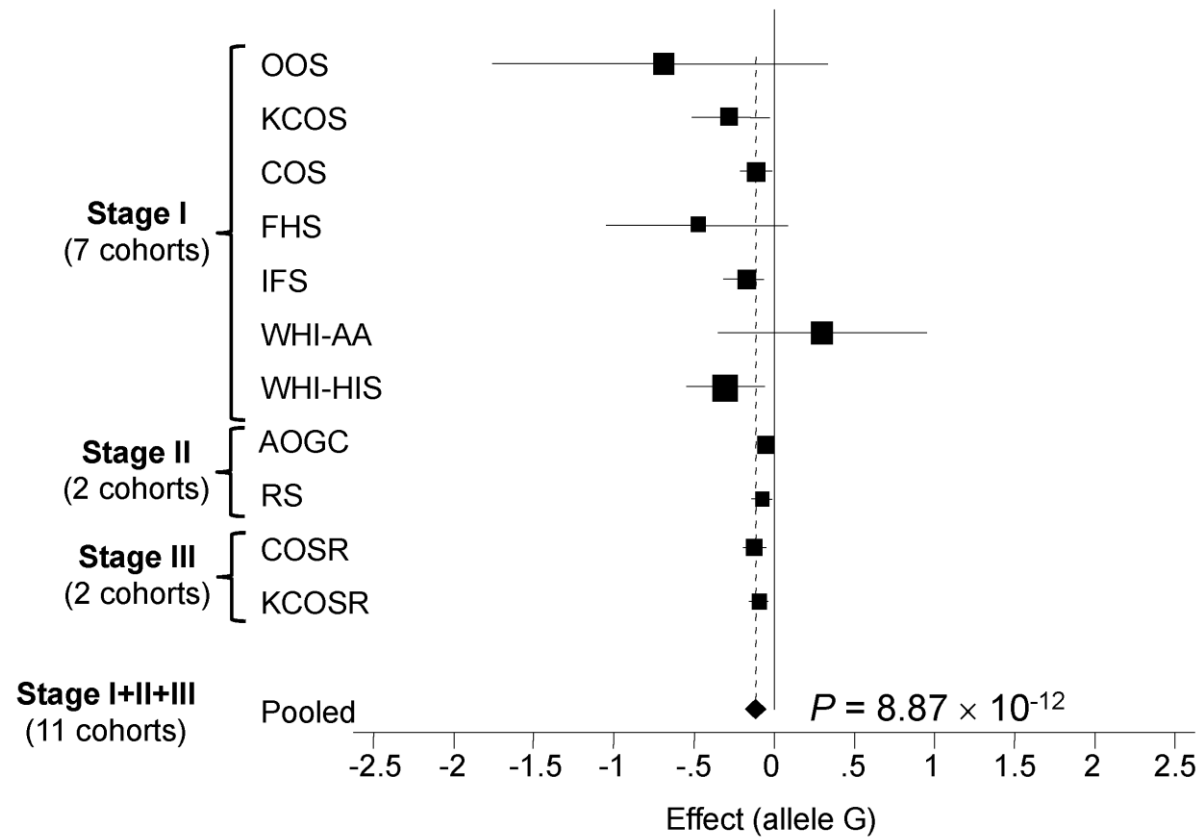


Figure 3

(A)

Chromosome 4p16.3

(B)

Chromosome 4p16.3
(Zoom-in View)

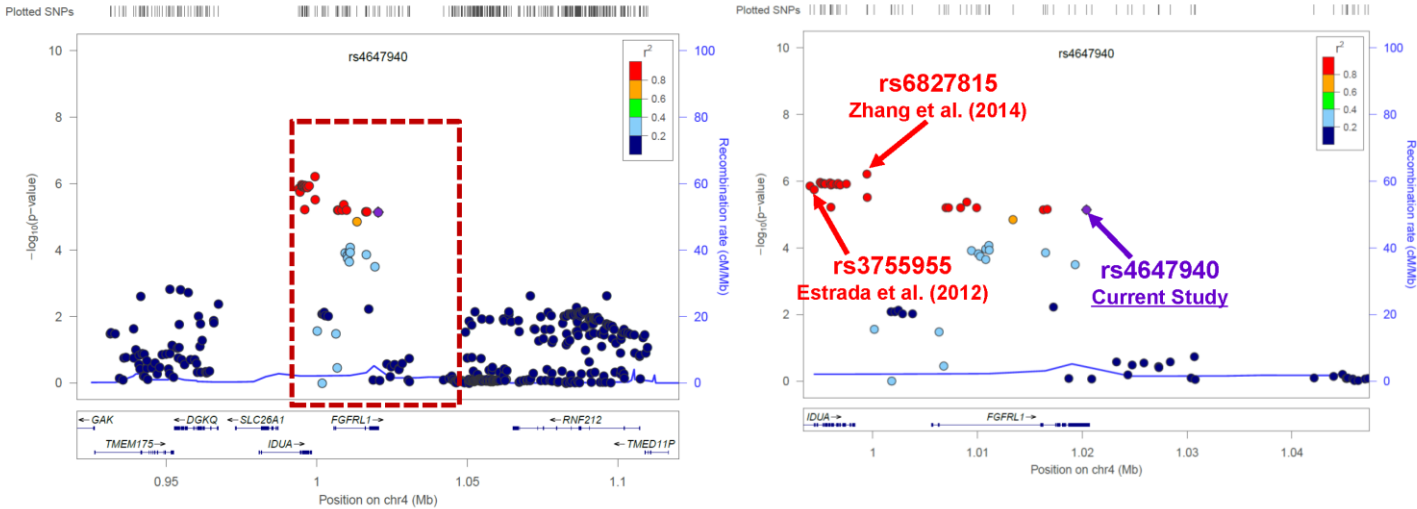
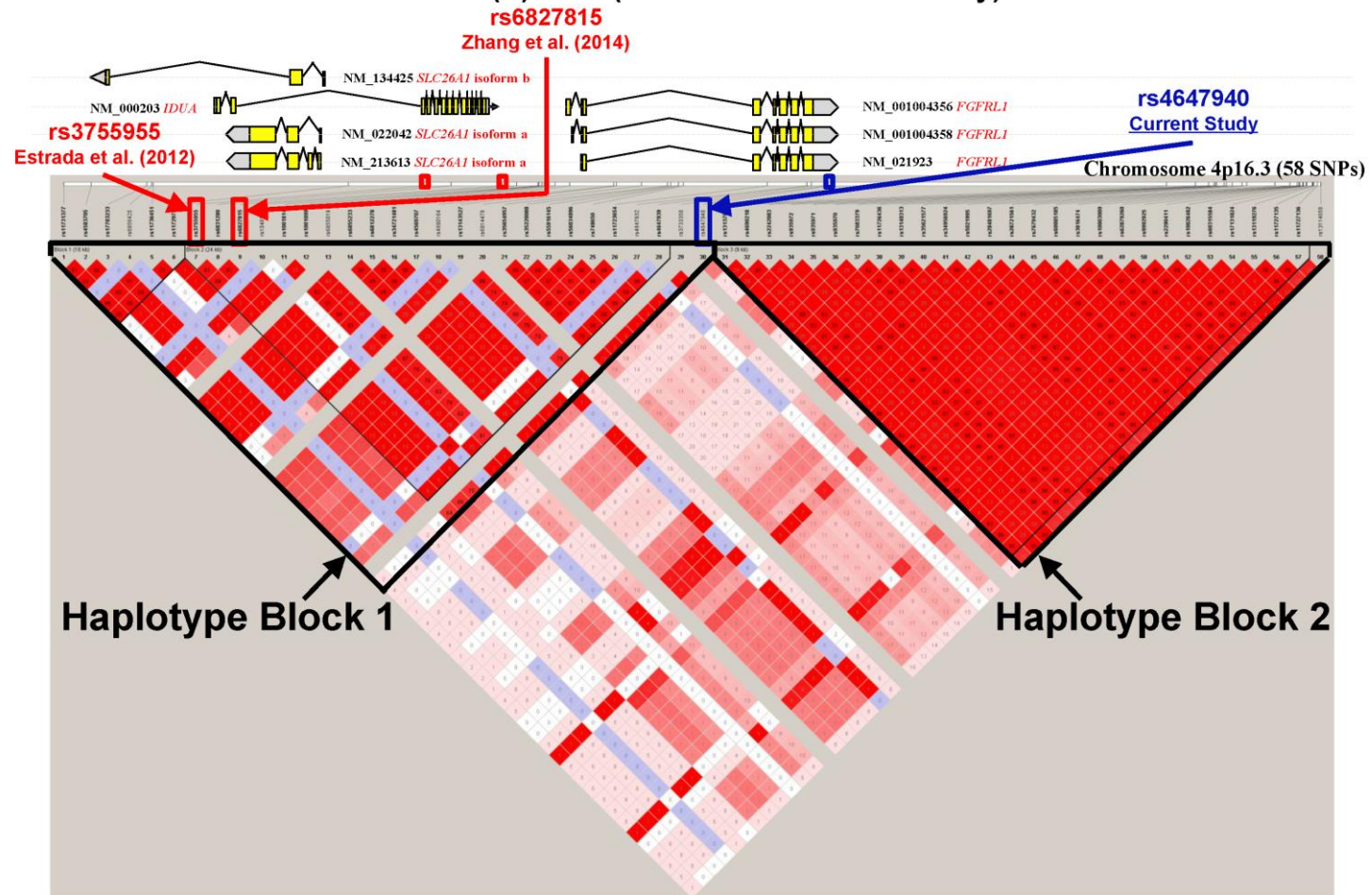


Figure 4

(A) OOS ($N=987$ Caucasian Ancestry)

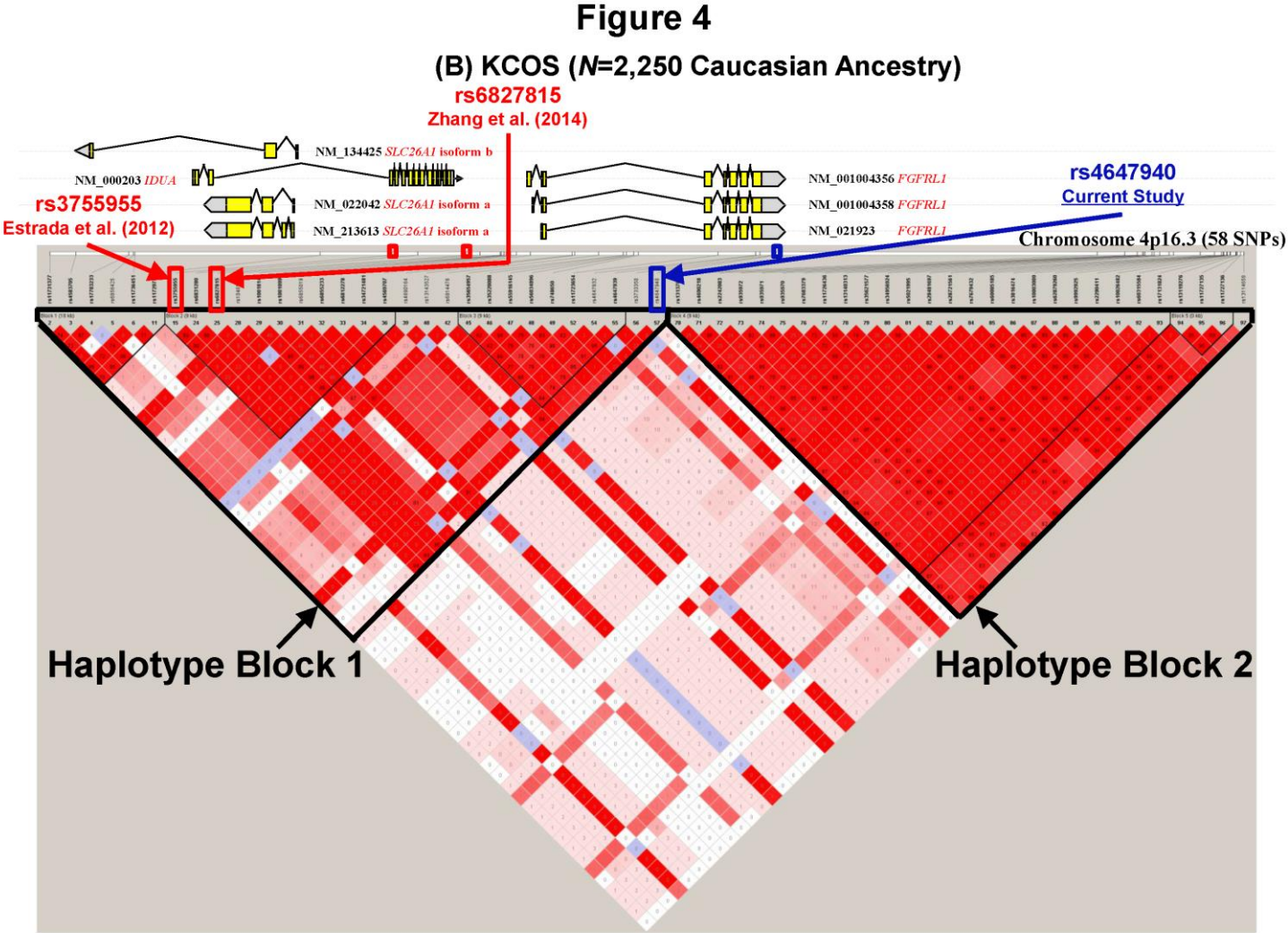


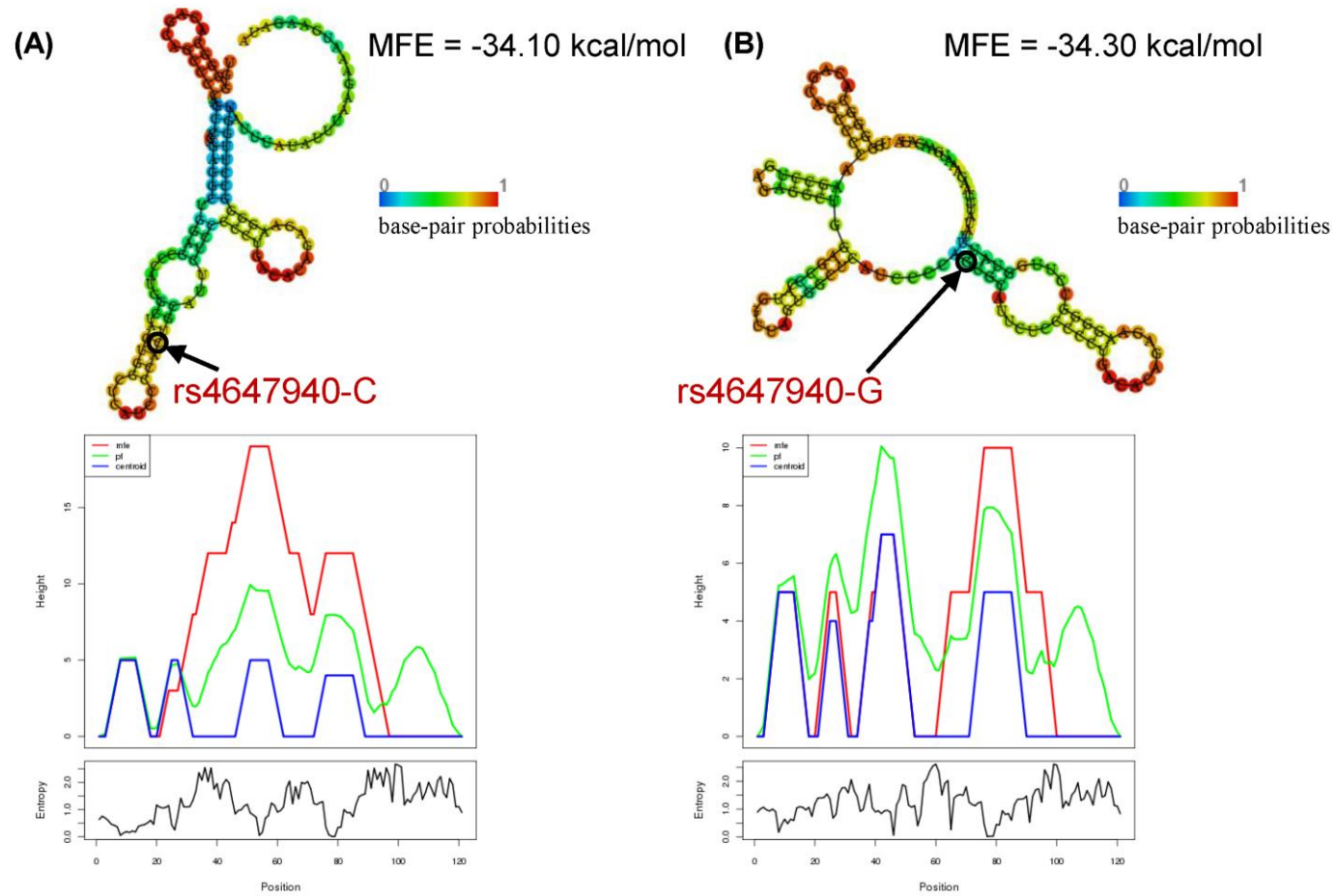
Figure 5

Figure 7

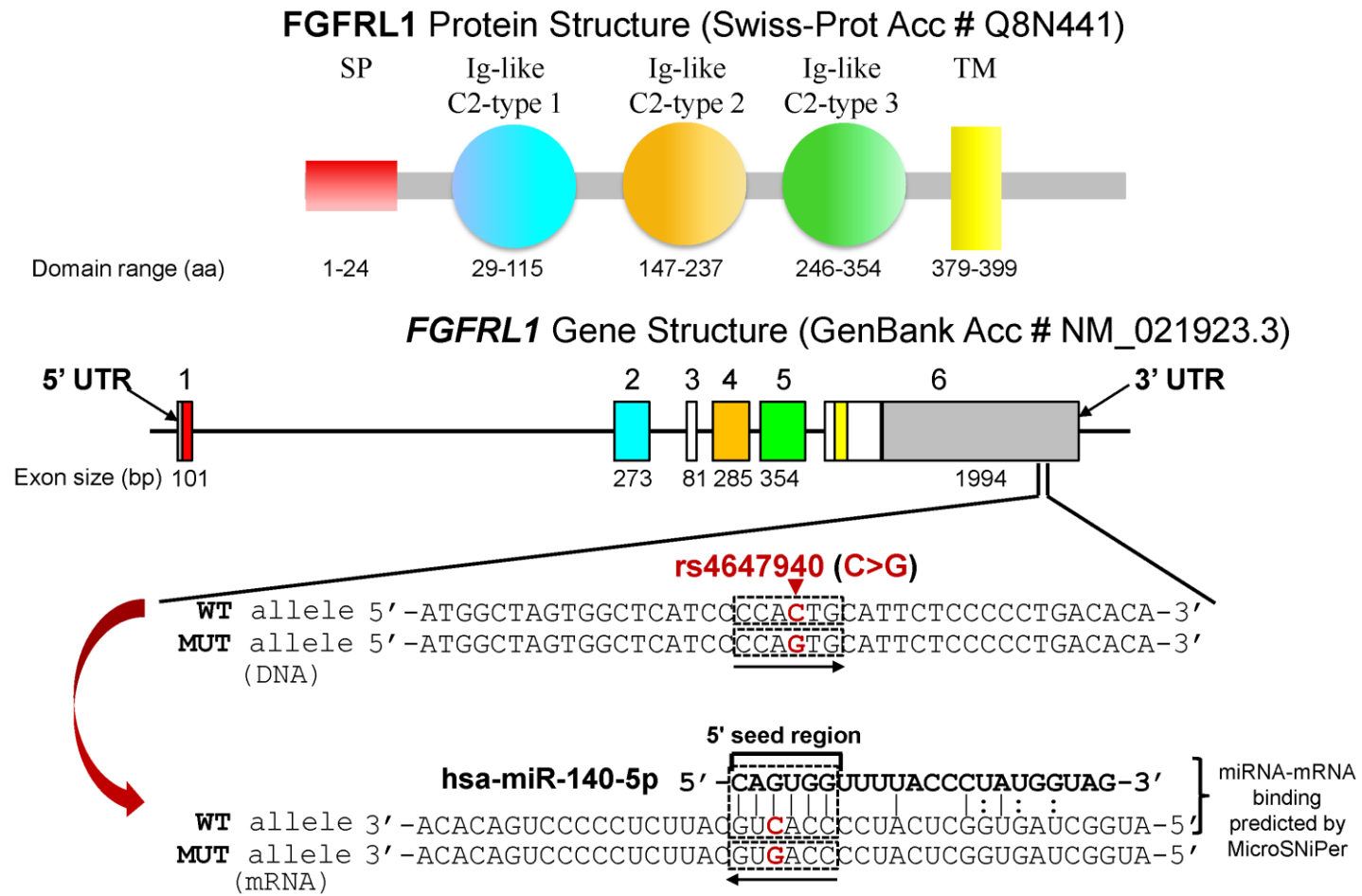


Figure 8

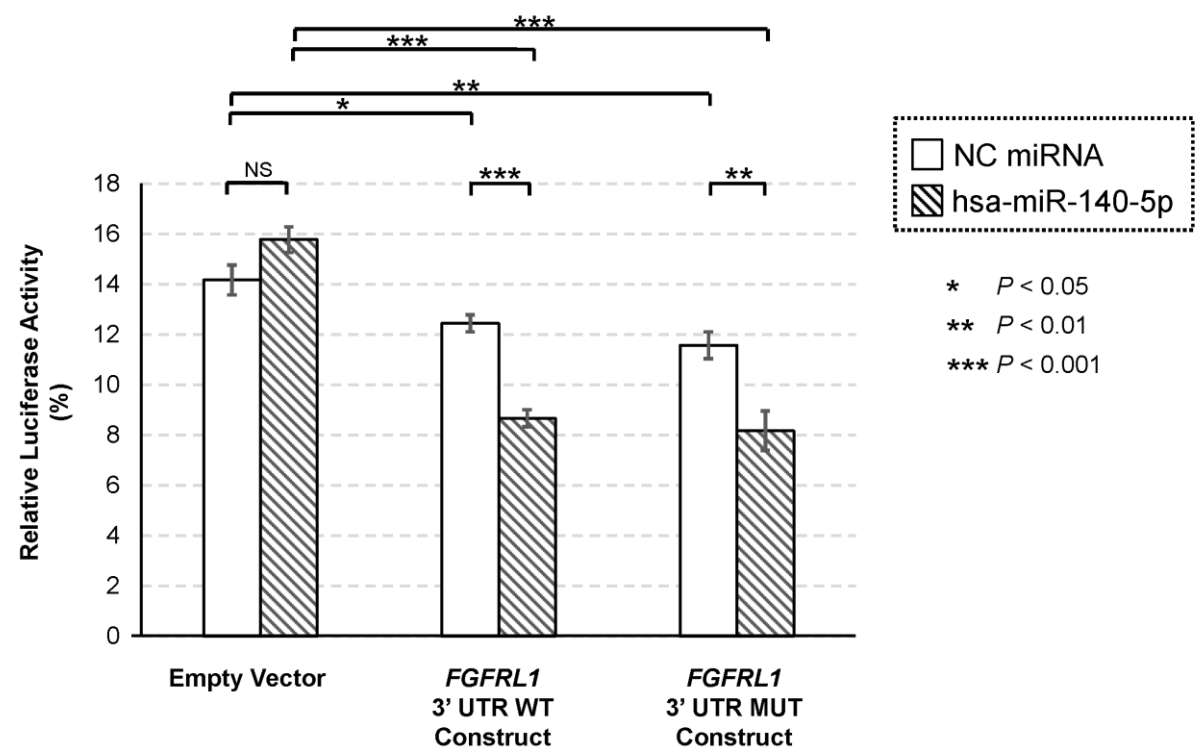


Figure 9

